Government of Canada Gouvernement du Canada

Canada

Experimental and Numerical Studies of the Effects of Upper Surface Roughness on Aileron Performance

TP 14180E

November 2003

Prepared for
Transportation Development Centre
Safety and Security
Transport Canada

by

Aerodynamics Laboratory
Institute for Aerospace Research
National Research Council Canada
Ottawa, Ontario

TP14180E

Experimental and Numerical Studies of the Effects of Upper Surface Roughness on Aileron Performance

by

P.J. Penna, J.C. Su and G.F. Syms

Aerodynamics Laboratory
Institute for Aerospace Research
National Research Council Canada
Ottawa, Ontario

November 2003

This report reflects the views of the authors and not necessarily those of the Transportation Development Centre of Transport Canada.

The Transportation Development Centre does not endorse products or manufacturers. Trade or manufacturer's names appear in this report only because they are essential to its objectives.

Since some of the accepted measures in the industry use Imperial Units, these have been provided in parentheses next to their equivalent value in S.I. Units.

This report was prepared by members of the staff of the Institute for Aerospace Research, National Research Council Canada and is based on a paper presented by the authors at the FAA In-flight Icing / Ground De-icing International Conference & Exhibition, Chicago, Illinois, June 16-20, 2003. Additional material that was not presented in the paper has been included to provide a more complete discussion of the aerodynamic effects of roughness that simulates the failure of anti-icing fluid by freezing precipitation.

Project Team

P.J. Penna

J.C. Su

G.F. Syms

Research Officers

Aerodynamics Laboratory

Institute for Aerospace Research

National Research Council Canada

Un sommaire français se trouve avant la table des matières.

Transport Canada / Transports Canada

PUBLICATION DATA FORM

1. Transport Canada Publication No.	2. Project No.	3. Recipient's Catalogue No.
TP 14180E	5201	

4. Title and Subtitle

Experimental and Numerical Studies of the Effects of Upper Surface Roughness on Aileron Performance

5. Publication Date

November 2003

6. Performing Organization Document No.

7. Author(s)

P.J. Penna, J.C. Su, and G.F. Syms

8. Transport Canada File No.

DC1962450B14ZCD

9. Performing Organization Name and Address

Aerodynamics Laboratory
Institute for Aerospace Research
National Research Council Canada
Ottawa, Ontario
Canada K1A 0R6

10. PWGSC File No.

11. PWGSC or Transport Canada Contract No.

12. Sponsoring Agency Name and Address

Transportation Development Centre (TDC)
800 René Lévesque Blvd. West
Suite 600
Montreal, Quebec
H3B 1X9

13. Type of Publication and Period Covered

Final

14. Project Officer

Barry B. Myers

15. Supplementary Notes (Funding programs, titles of related publications, etc.)

This report has also been published by National Research Council Canada as Laboratory Technical Report LTR-AL-2003-0097.

16. Abstract

Experimental and numerical studies were conducted to quantify the aerodynamic degradation resulting from the presence of failed anti-icing fluid on the upper surface of aircraft wings.

Wind tunnel tests were conducted on an un-swept wing of an NACA 4415 section with selected roughness profiles applied to the leading edge, ahead of the aileron, with the same span-wise length as the aileron.

Calculations were conducted for a two-dimensional NACA 4415 airfoil with aileron, a Fokker F-28 aircraft, an NASA LS(1)-0417 airfoil with a flap, and the NACA 4415 wing-aileron studied in the wind tunnel, all with varying amounts of simulated roughness.

Numerical study results were consistent with experimental observations.

In the cases studied, decreasing the chord-wise extent of the roughness had little influence on the magnitude of lift loss; presence of roughness at the leading edge reduced the stall angle of attack by as much as 4 degrees; lift loss was more pronounced for a downward aileron deflection than for an upward aileron deflection; and increasing aileron deflection produced an increasing reduction in maximum lift beyond stall.

The roughness distributions studied, if applied to only one wing combined with an attempt to rotate the aircraft to its maximum allowable angle of attack at takeoff, could result in a significant loss of lift on the wing together with loss of aileron effectiveness.

17. Key Words	18. Distribution Statement
Aerodynamic roughness effects, wind tunnel tests, computational fluid dynamics, aileron effectiveness	Limited number of copies available from the Transportation Development Centre

19. Security Classification (of this publication)	20. Security Classification (of this page)	21. Declassification (date)	22. No. of Pages	23. Price
Unclassified	Unclassified	—	xviii, 38	Shipping/ Handling

Transports Canada Transport Canada

FORMULE DE DONNÉES POUR PUBLICATION

1. N° de la publication de Transports Canada	2. N° de l'étude	3. N° de catalogue du destinataire
TP 14180E	5201	

4. Titre et sous-titre	5. Date de la publication
Experimental and Numerical Studies of the Effects of Upper Surface Roughness on Aileron Performance	Novembre 2003
	6. N° de document de l'organisme exécutant

7. Auteur(s)	8. N° de dossier - Transports Canada
P.J. Penna, J.C. Su et G.F. Syms	DC1962450B14ZCD

9. Nom et adresse de l'organisme exécutant	10. N° de dossier - TPSGC
Laboratoire d'aérodynamique Institut de recherche aérospatiale Conseil national de recherches du Canada Ottawa, Ontario Canada K1A 0R6	11. N° de contrat - TPSGC ou Transports Canada

12. Nom et adresse de l'organisme parrain	13. Genre de publication et période visée
Centre de développement des transports (CDT) 800, boul. René-Lévesque Ouest Bureau 600 Montréal (Québec) H3B 1X9	Final
	14. Agent de projet Barry B. Myers

15. Remarques additionnelles (programmes de financement, titres de publications connexes, etc.)

Ce rapport a aussi été publié par le Conseil national de recherches du Canada sous le numéro LTR-AL-2003-0097.

16. Résumé

Des études expérimentales et numériques ont été menées pour mesurer la dégradation de l'aérodynamique d'une aile d'avion résultant de la présence de fluide antigivre contaminé sur son extrados.

Une aile droite de profil NACA 4415 a été soumise à des essais en soufflerie. Divers profils de rugosité étaient apposés sur le bord d'attaque, en avant de l'aileron. Leur longueur était équivalente à l'envergure de l'aileron.

Les études numériques ont porté sur une surface portante bidimensionnelle NACA 4415 avec aileron, un avion Fokker F-28, une surface portante NASA LS(1)-0417 avec volet, et le profil d'aile NACA 4415 avec aileron étudié dans la soufflerie, présentant tous des degrés variables de rugosité simulée.

Les résultats des études numériques coïncident avec les observations expérimentales.

Dans les cas étudiés, le fait de diminuer l'étendue de la rugosité dans le sens de la corde avait peu d'effet sur la perte de portance; la présence de rugosités sur le bord d'attaque réduisait d'une valeur pouvant aller jusqu'à 4 degrés l'angle d'attaque de décrochage; l'abaissement de l'aileron entraînait une perte de portance plus prononcée que son soulèvement; et plus l'aileron était braqué, plus la portance maximale diminuait, passé le point de décrochage.

Si les distributions de rugosités étudiées étaient apposées sur une seule aile et que l'avion était cabré jusqu'à l'angle d'attaque maximal permis pour le décollage, il pourrait s'ensuivre une perte de portance importante de l'aile en même temps qu'une perte d'efficacité de l'aileron.

17. Mots clés	18. Diffusion
Effets de la rugosité sur l'aérodynamique, essais en soufflerie, dynamique computationnelle des fluides, efficacité des ailerons	Le Centre de développement des transports dispose d'un nombre limité d'exemplaires.

19. Classification de sécurité (de cette publication)	20. Classification de sécurité (de cette page)	21. Déclassification (date)	22. Nombre de pages	23. Prix
Non classifiée	Non classifiée	—	xviii, 38	Port et manutention

ACKNOWLEDGEMENTS

This work was supported by Transportation Development Centre of Transport Canada. The authors would like to thank Messrs. Frank Eyre and Barry Myers for their helpful discussions and cooperation. Thanks are also due to Drs. Norman Ball and Myron Oleskiw of NRCC for their invaluable discussions and efforts.

EXECUTIVE SUMMARY

Experimental and numerical studies were conducted to quantify the aerodynamic penalties resulting from the presence of failed anti-icing fluid on the upper surface of aircraft wings. The experimental study consisted of a wind tunnel test of a reflection-plane wing with a rectangular plan form and an aspect ratio of 5.3 when reflected. The wing was un-twisted and had an NACA 4415 airfoil section with a 30 percent of chord aileron. The test Reynolds number and Mach number were 3×10^6 and 0.3, respectively. Three sizes of distributed roughness, with elemental height-to-chord ratios of 0.0003, 0.0005 and 0.0006, were sequentially applied to the upper surface of the wing and all roughness applications commenced at the leading edge of the wing, upstream of the aileron only. The roughness therefore covered only part of the wing span and extended from the leading edge to either 2, 15 or 30 percent of chord. The roughness characteristics and coverage were chosen to represent a local region of failed anti-icing fluid that had resulted from exposure to freezing precipitation prior to takeoff.

The first numerical study consisted of a viscous-flow analysis of the corresponding two-dimensional NACA 4415 airfoil with a 30 percent of chord aileron. The study was carried out using the Navier-Stokes CFD solver, NPARC. The two-equation k-ω turbulence model was used without wall functions in NPARC as it allowed the specification of a surface roughness. A second numerical study examined the flow about three geometries: a Fokker F-28 MK1000 aircraft with aileron deflections, an NASA LS(1)-0417 airfoil with a flap and the three-dimensional NACA 4415 wing with an aileron that was used in the experimental study. These three geometries were investigated using the three-dimensional, potential/viscous interaction solver of the Aerodynamics Laboratory, PMAL3D. For the NASA LS(1)-0417 airfoil with flap, actual experimental results were available for comparison. These were from an earlier National Research Council Canada-Institute for Aerospace Research (NRCC-IAR) wind tunnel investigation that documented the aerodynamic effects of actual failed fluids resulting from snow contamination.

The experimental wind tunnel study of the NACA 4415 wing with an aileron showed that the presence of roughness always produced a reduction in maximum lift coefficient and stall angle of attack. The magnitudes of these penalties were influenced by:

- roughness height;
- extent of roughness coverage of the wing; and
- non-dimensional spacing of roughness elements.

Greater non-dimensional spacing of roughness elements prevented an increase in the aerodynamic penalty usually associated with greater roughness height. On the other hand, reducing the extent of roughness coverage from 30 to 2 percent of chord did not lead to a proportional change in aerodynamic penalties for roughness having an elemental height-to-chord ratio of 0.0005 and the smallest non-dimensional spacing. Depending on the aileron setting, reduction in maximum lift was still 12 to 15 percent for roughness coverage to 2 percent of chord, compared to an 18 to 23 percent reduction in maximum lift for roughness coverage to 30 percent of chord.

By applying the experimental reductions in maximum lift to a hypothetical aircraft using this wing, it was possible to convert each reduction to an equivalent increase in the aircraft's 1 *g* stall speed with aileron neutral. Coverage extending to 30 percent of chord of the roughness having an elemental height-to-chord ratio of 0.0005 and the smallest non-dimensional spacing was the most detrimental. Stall speed increased by 13 percent, equal to the typical stall speed safety margin used to determine the takeoff speed for modern transport aircraft. In other words, the wing would stall if the hypothetical aircraft attempted takeoff at the normal specified speed. The same conclusion was reached when this roughness extended to only 15 percent of chord, but with a slightly reduced stall speed safety margin of 10 percent.

Where appropriate, experimental results for the NACA 4415 wing and the NASA LS(1)-0417 airfoil were compared to those from the two and three-dimensional numerical calculations. Generally, the numerical studies were consistent with the experiments and showed comparable reductions in maximum lift and stall angle of attack.

Both experimental and numerical studies showed that roughness on an aircraft's wing at takeoff could have a negative impact on controllability. If a localized area of failed fluid goes undetected during the inspection prior to takeoff, its roughness could reduce the aircraft's roll-control at the completion of aircraft rotation, when the angle of attack is increased to initiate lift-off from the runway. Roughness could cause the wing to stall before it reaches the clean-wing stall angle of attack and a stall could occur if an attempt is made to rotate the aircraft very close to this angle of attack. In this scenario, it is expected that the undetected area of the roughness is small relative to the total wing area, but the roughness could be located on or near the leading edge, possibly on one wing only and ahead of an aileron. The extent of roughness coverage could be represented by the smallest studied here (2 percent of chord), resulting in a 2 to 4 degree reduction in stall angle of attack for the experimental NACA 4415 wing. If this roughness is present on only one wing during takeoff, and an attempt is made to rotate the aircraft to within a few degrees of its clean-wing stall angle of attack, the roughness could induce a localized premature flow separation leading to a significant loss of lift on the roughened wing. This study shows that along with a stalled wing, there is a compounding problem of loss of aileron effectiveness, occurring at a time when normal roll control is required to correct the resulting un-commanded roll towards the compromised wing.

For an operational aircraft exposed to freezing precipitation on the ground, the larger extents of roughness coverage studied here (15 and 30 percent of chord), when translated into equivalent extents of failed fluid, should be large enough for detection during a normal inspection prior to takeoff. Regulatory authorities require that all roughness be removed from the wing prior to takeoff. Even though the larger extents of roughness should be absent during takeoff, they were included in these studies to investigate the effect that changes in extent of coverage had on the magnitude of aerodynamic penalties. These studies are expected to provide a reference for future work.

SOMMAIRE

Des études expérimentales et numériques ont été menées pour mesurer la dégradation de l'aérodynamique d'une aile d'avion résultant de la présence de fluide antigivre contaminé sur son extrados. L'étude expérimentale consistait en un essai en soufflerie d'une aile à plan de symétrie présentant une forme plane rectangulaire et un allongement de 5,3, lorsque réfléchie. L'aile était sans torsion et arborait le profil NACA 4415, avec un aileron équivalent à 30 p. 100 de la corde. Le nombre de Reynolds et le nombre de Mach réalisés au cours des essais étaient de 3×10^6 et 0,3 respectivement. Des bandes de rugosité distribuée présentant des rapports de l'épaisseur des rugosités à la corde de 0,0003, 0,0005 et 0,0006 ont été successivement appliquées sur l'extrados de l'aile. Toutes partaient du bord d'attaque et se limitaient à la surface en amont de l'aileron. Ainsi, les rugosités ne couvraient qu'une partie de l'envergure de l'aile et s'étendaient, à partir du bord d'attaque, sur une distance équivalant à 2, 15 ou 30 p. 100 de la corde. Les caractéristiques des rugosités et les degrés de couverture ont été choisis de façon à représenter la contamination de zones limitées de fluide antigivre par suite d'une exposition à des précipitations givrantes avant le décollage.

La première étude numérique a consisté en une analyse de l'écoulement visqueux autour de la surface portante NACA 4415 bidimensionnelle correspondant à l'aile étudiée en soufflerie, avec un aileron mesurant 30 p. 100 de la corde. L'étude a été réalisée à l'aide du code Navier-Stokes NPARC. Le modèle de turbulence à deux équations k-ω a été utilisé sans les lois de paroi du NPARC, car il permettait de préciser une rugosité de la surface. Une deuxième analyse numérique a porté sur l'écoulement autour de trois géométries : un avion Fokker F-28 MK1000 avec différents angles de braquage de l'aileron, une surface portante NASA LS(1)-0417 avec un volet et le profil d'aile NACA 4415 tridimensionnel avec aileron qui avait servi aux essais en soufflerie. Ces trois géométries ont été étudiées à l'aide du code tridimensionnel d'interaction entre écoulement potentiel non visqueux et couche limite visqueuse (PMAL3D) mis au point par le laboratoire d'aérodynamique. Pour la surface portante NASA LS(1)-0417 avec volet, des résultats d'expériences en vraie grandeur étaient disponibles pour comparaison. Ils étaient issus d'une étude antérieure menée en soufflerie par l'Institut de recherche aérospatiale du Conseil national de recherches du Canada (IRA-CNRC), qui documentait les effets aérodynamiques de fluides réels contaminés par de la neige.

L'étude en soufflerie du profil d'aile NACA 4415 avec aileron a révélé que la présence de rugosités entraîne toujours une diminution du coefficient de portance maximal et de l'angle d'attaque de décrochage. L'ampleur de ces effets était fonction de :

- l'épaisseur de la rugosité;
- la superficie couverte par la rugosité;
- l'espacement non dimensionnel des rugosités.

Un espacement non dimensionnel plus grand des rugosités faisait en sorte d'inhiber la diminution des performances aérodynamiques habituellement associées à une plus grande épaisseur des rugosités. Par contre, le fait de porter de 30 à 2 p. 100 de la corde la couverture des rugosités n'a pas mené à une dégradation proportionnelle de

l'aérodynamique dans le cas où les rugosités présentaient un rapport de l'épaisseur à la corde de 0,0005 et où l'espacement non dimensionnel était le plus faible. Selon l'angle de braquage de l'aileron, la réduction de la portance maximale était de 12 à 15 p. 100, lorsque la rugosité couvrait 2 p. 100 de la corde, comparativement à une réduction de 18 à 23 p. 100, lorsque la rugosité couvrait 30 p. 100 de la corde.

En appliquant les pertes de portance maximale dérivées des essais à un avion hypothétique équipé de l'aile étudiée, il a été possible de convertir chaque diminution de portance en une augmentation équivalente de la vitesse de décrochage 1 *g*, avec aileron neutre. Le cas de figure le plus préjudiciable était celui où les rugosités couvraient 30 p. 100 de la corde, où le rapport de l'épaisseur des rugosités à la corde était de 0,0005 et où l'espacement non dimensionnel était le plus faible. La vitesse de décrochage augmentait alors de 13 p. 100, ce qui correspond à la marge de sécurité habituellement utilisée pour déterminer la vitesse pour le décollage des avions de transport modernes. Autrement dit, l'aile «décrocherait» si l'avion hypothétique tentait un décollage à la vitesse normale prescrite. Cette conclusion valait aussi pour le cas où la rugosité s'étendait sur seulement 15 p. 100 de la corde, mais la marge de sécurité concernant la vitesse de décrochage était alors un peu plus mince, soit 10 p. 100.

Lorsque les données s'y prêtaient, les résultats expérimentaux obtenus avec le profil d'aile NACA 4415 et la surface portante NASA LS(1)-0417 ont été comparés à ceux issus des calculs numériques bidimensionnels et tridimensionnels. En général, les deux ensembles de résultats concordaient, révélant des diminutions comparables de la portance maximale et de l'angle d'attaque de décrochage.

Tant les essais en soufflerie que les études numériques ont révélé que la présence de rugosités sur l'aile d'un avion au décollage pourrait avoir un effet négatif sur la manœuvrabilité. Si la présence de fluide contaminé sur une partie de l'aile échappe à l'inspection avant le décollage, cette rugosité réduira la commande en roulis de l'avion à la fin de sa rotation, lorsque le pilote augmentera l'angle d'attaque pour amorcer le décollage de la piste. La rugosité pourrait faire en sorte que l'aile décroche avant que soit atteint l'angle d'attaque de décollage d'une aile propre, et l'avion pourrait entrer en décrochage si le pilote tentait de donner à l'avion un angle très près de cet angle d'attaque. Dans ce scénario, la surface rugueuse non détectée est peu étendue par rapport à la superficie totale de l'aile, mais elle pourrait être située sur le bord d'attaque ou à proximité, sur une seule aile, et en avant d'un aileron. Ce cas pourrait correspondre à l'essai mettant en jeu la plus faible superficie (2 p. 100 de la corde), qui a entraîné une réduction de 2 à 4 degrés de l'angle d'attaque de décrochage pour le profil d'aile NACA 4415. Si les rugosités couvrent une seule aile durant le décollage, et que le pilote augmente l'incidence jusqu'à s'approcher à quelques degrés de l'angle d'attaque de décrochage défini pour l'avion à voilure propre, la rugosité pourrait induire un décollement prématuré et localisé, qui entraînerait à son tour une importante perte de portance du côté de l'aile rugueuse. L'étude a montré qu'à une aile «décrochée» s'ajoute un problème de perte de l'efficacité de l'aileron, qui survient au moment où les commandes de roulis sont normalement nécessaires pour corriger le roulis intempestif vers l'aile rugueuse.

Pour un avion en service exposé à des précipitations givrantes au sol, les cas de couverture importante de la rugosité étudiés ici (15 et 30 p. 100 de la corde), lorsque

transposés en étendues équivalentes de fluide contaminé, ne devraient pas, normalement, échapper à l'inspection avant le décollage. Les organismes de réglementation exigent que les ailes soient débarrassées de toute rugosité avant qu'un avion puisse décoller. Même si la présence d'étendues importantes de rugosités pendant le décollage est peu plausible, ces cas ont quand même été analysés, car ils permettaient d'étudier l'influence de la surface couverte par les rugosités sur l'ampleur de la dégradation de l'aérodynamique. Les résultats obtenus devraient servir de référence à des travaux futurs.

TABLE OF CONTENTS

1. INTRODUCTION 1

2. EXPERIMENTAL STUDIES 2

2.1 Description of Experiments 2

2.2 Discussion of Experimental Results 3

2.3 Effect of Roughness on Aircraft Stall Speed 5

2.4 Effect of Roughness on Pressure Distribution and Roll Control 7

3. NUMERICAL STUDIES 7

3.1 Two-Dimensional Navier-Stokes Analysis 7

3.1.1 Discussion of Two-Dimensional Navier-Stokes Results 8

3.2 Three-Dimensional Viscous Analysis 9

3.2.1 Discussion of Three-Dimensional Viscous Results 9

4. CONCLUSIONS 12

FIGURES 15

REFERENCES 37

LIST OF FIGURES

Figure 1a Wind tunnel model dimensions (mm) 15

Figure 1b Wind tunnel model with roughness to 0.02c; δ = -20° 16

Figure 2 Roughness; k/c = 0.0006 to 0.15c; λ = 140 17

Figure 3 Experimental C_L vs. α; NACA 4415 wing-aileron; δ = 0° 18

Figure 4 Experimental C_L vs. α; NACA 4415 wing-aileron; δ = 10° 18

Figure 5 Experimental C_L vs. α; NACA 4415 wing-aileron; δ = 20° 19

Figure 6 Experimental C_L vs. α; NACA 4415 wing-aileron; δ = -10° 19

Figure 7 Experimental C_L vs. α; NACA 4415 wing-aileron; δ = -20° 20

Figure 8 Experimental reduction in α_s 20

Figure 9 Experimental reduction in C_{Lmax} 21

Figure 10 Experimental C_p vs. x/c; δ = 0° 21

Figure 11 Experimental C_p vs. x/c; δ = 20° 22

Figure 12 Experimental ΔC_l vs. δ 22

Figure 13 2-D NS C_L vs. α; NACA 4415 airfoil; clean surface 23

Figure 14 2-D NS C_L vs. α; NACA 4415 airfoil; δ = 0°; clean and rough surface 23

Figure 15 2-D NS reduction in C_{Lmax}; NACA 4415 airfoil; δ = 0° 24

Figure 16 2-D NS reduction in C_{Lmax}; NACA 4415 airfoil; roughness to 0.3c 24

Figure 17 Surface paneling for Fokker F-28 MK1000 aircraft 25

Figure 18 C_L vs. α; Fokker F-28; δ = 0°; 18° flap; Re = 17.5 x 10^6 25

Figure 19 C_L vs. α; Fokker F-28; 18° flap; potential solution 26

Figure 20 C_L vs. α; Fokker F-28; 18° flap; viscous solution; clean surface 26

Figure 21 C_L vs. α; Fokker F-28; 18° flap; potential and viscous solutions 27

Figure 22 C_L vs. α; Fokker F-28; 18° flap; clean and rough viscous solutions 27

Figure 23 C_L vs. α; NASA LS(1)-0417 configuration; 15° flap; Re = 5 x 10^6 28

Figure 24 C_L vs. α; NACA 4415 airfoil; clean surface; Re = 3.2 x 10^6 28

Figure 25a C_L vs. α; NACA 4415 wing; δ = 0°; Re = 3.2 x 10^6 29
Figure 25b C_L vs. α; NACA 4415 wing; δ = -10°; Re = 3.2 x 10^6 29
Figure 25c C_L vs. α; NACA 4415 wing; δ = 10°; Re = 3.2 x 10^6 30
Figure 26a C_p vs. *x/c;* NACA 4415 wing; *y/b* = 0.63; δ = 0°; α = -4.06° 30
Figure 26b C_p vs. *x/c;* NACA 4415 wing; *y/b* = 0.81; δ = 0°; α = -4.06° 31
Figure 26c C_p vs. *x/c;* NACA 4415 wing; *y/b* = 0.63; δ = 0°; α = 2.18° 31
Figure 26d C_p vs. *x/c;* NACA 4415 wing; *y/b* = 0.81; δ = 0°; α = 2.18° 32
Figure 27a C_p vs. *x/c;* NACA 4415 wing; *y/b* = 0.63; δ = -10°; α = -4.15° 32
Figure 27b C_p vs. *x/c;* NACA 4415 wing; *y/b* = 0.81; δ = -10°; α = -4.15° 33
Figure 27c C_p vs. *x/c;* NACA 4415 wing; *y/b* = 0.63; δ = -10°; α = 2.07° 33
Figure 27d C_p vs. *x/c;* NACA 4415 wing; *y/b* = 0.81; δ = -10°; α = 2.07° 34
Figure 28a C_p vs. *x/c;* NACA 4415 wing; *y/b* = 0.63; δ = 10°; α = -3.95° 34
Figure 28b C_p vs. *x/c;* NACA 4415 wing; *y/b* = 0.81; δ = 10°; α = -3.95° 35
Figure 28c C_p vs. *x/c;* NACA 4415 wing; *y/b* = 0.63; δ = 10°; α = 2.27° 35
Figure 28d C_p vs. *x/c;* NACA 4415 wing; *y/b* = 0.81; δ = 10°; α = 2.27° 36

LIST OF TABLES

Table 1 Roughness geometric parameters.....3
Table 2 Increase in stall speed due to roughness.....6

GLOSSARY OF ABBREVIATIONS

AEDC	Arnold Engineering Development Center, Department of Defense
CFD	Computational Fluid Dynamics
FAA	Federal Aviation Administration
FAR	Federal Aviation Regulations
IAR	Institute for Aerospace Research of NRCC
NACA	National Advisory Committee for Aeronautics
NASA	National Aeronautics and Space Administration
NPARC	NS CFD Solver from NASA-AEDC
NRCC	National Research Council Canada
NS	Navier-Stokes
PMAL3D	Panel Method, Aerodynamics Laboratory, Three-Dimensional
PMARC	Panel Method of the NASA Ames Research Center
2-D	Two-Dimensional
3-D	Three-Dimensional

LIST OF SYMBOLS

a	Speed of sound in air
A_F	Frontal area of a typical individual roughness element
b	Wing span
c	Wing chord
C_L	Lift coefficient, $\frac{L}{\frac{1}{2}\rho V_\infty^2 S}$
C_{Lmax}	Maximum lift coefficient
C_l	Rolling moment coefficient, $\frac{RM}{\frac{1}{2}\rho V_\infty^2 Sb}$
ΔC_l	Change in C_l produced by aileron deflection for a semi-span wing
C_p	Surface pressure coefficient, $\frac{p - p_\infty}{\frac{1}{2}\rho V_\infty^2}$
D^2	Average surface area occupied by a roughness element
g	Acceleration due to gravity

k Height of a typical roughness element; turbulent kinetic energy in NPARC

L Lift

M Mach number, $\frac{V}{a}$

p Surface pressure on wing

p_∞ Free-stream static pressure

R Fractional reduction in maximum lift coefficient, $\frac{(C_{L\max-c} - C_{L\max-r})}{C_{L\max-c}}$

RM Rolling moment

Re Reynolds number based on wing reference chord, $\frac{Vc}{\upsilon}$

S Wing area

V Wind speed; true airspeed for an aircraft

W Weight of an aircraft

x Coordinate measured along the chord of the wing (x = 0 at the leading edge)

y Coordinate measured along the span of the wing (y = 0 at the root)

y^+ Non-dimensional distance to wall

α Angle of attack

δ Aileron deflection, positive trailing edge down

λ Average non-dimensional spacing between roughness elements

ρ Air density

υ Kinematic viscosity of air

ω Specific dissipation rate

List of Subscripts

c Clean, without roughness present

r With roughness present

s Stall

∞ Free-stream conditions

1. INTRODUCTION

In collaboration with the Transportation Development Centre (TDC) of Transport Canada, the Institute for Aerospace Research (IAR) of the National Research Council of Canada (NRCC) carried out wind tunnel tests and developed numerical techniques designed to observe and predict the effect of upper surface roughness on the performance of a wing with an aileron. These studies were part of a continuing program to quantify the aerodynamic degradation resulting from the presence of failed anti-icing fluid on significant portions of the upper surface of aircraft wings [1-5]. A recent, comprehensive review by Lynch and Khodadoust [6] of a wide range of public domain studies summarized the aerodynamic penalties (reductions in maximum lift and stall angle) resulting from the presence of roughness on two-dimensional airfoils and three-dimensional wings and tail planes. Most of the data presented in [6] addresses roughness effects due to in-flight icing or ground icing characterized by frost. However, an equally important problem is the aerodynamic effect of adhering slush resulting from localized failure of anti-icing fluid applied to protect the lifting surfaces of aircraft on the ground during exposure to freezing precipitation.

If a localized area of failed fluid goes undetected during the inspection prior to takeoff, its roughness could pose a hazard at takeoff and especially right at the point of aircraft rotation where the angle of attack is increased to initiate the lift-off from the runway. In this scenario, it is expected that the surface area of the roughness is small relative to the total wing area, but the roughness could be located on or near the leading edge, possibly on one wing only and ahead of an aileron. Hence, the roughness could induce a localized premature flow separation that would lead to loss of lift on only one wing, along with an un-commanded roll towards the compromised wing.

As mentioned above, there have been many public domain studies of the aerodynamic effects of both distributed roughness at the leading edge and gross discontinuities in leading edge profile (as produced by in-flight icing) for both two-dimensional airfoil sections and three-dimensional wings. The two-dimensional studies require, by the nature of their two-dimensionality, that roughness be uniform and continuous along the span of the airfoil, regardless of whether the study is experimental or computational. Furthermore, in three-dimensional studies of wings or tail planes, the roughness is usually uniform and continuous along the full span. There appear to be no studies of the aerodynamic effects of a small patch of adhering roughness covering only a fraction of the span of a three-dimensional wing, expressed as an area of roughness of given profile. While detailed, accurate measurements of the roughness profile of adhering slush are not available in the literature, the best available data suggests full-scale roughness heights of 0.5 to 1.0 mm, well above the threshold capabilities of available "contamination" sensors, designed specifically to detect failed i.e., contaminated, fluids. A single-point contamination sensor permanently installed on the wing (as opposed to one which surveys the total surface) could conceivably miss the presence of a small area of slush and therefore provide no warning to the pilot of a wing with roughness. Furthermore, no data are available defining the conditions under which slush adheres to a wing during the takeoff run. In order to err on the side of safety, it is therefore assumed that slush on the wing prior to takeoff will not be removed by aerodynamic shear stress

during the takeoff run before rotation is initiated. This assumption is the rationale for the regulatory requirement that all roughness be removed from aircraft lifting surfaces before take off.

In consideration of the foregoing, experimental and numerical studies were conducted to simulate the aerodynamic effects of localized roughness resulting from the presence of slush contamination on a wing with an aileron. For one of the geometries selected for study, the roughness was located upstream of the aileron and extended from the leading edge to 2, 15 or 30 percent of chord. Such convenient and extensive distributions of roughness (almost 50 percent of wing span, to match the span of the aileron) are, of course, not expected in every occurrence of ground icing and are unlikely to pass undetected, but were selected to provide reference for future work.

2. EXPERIMENTAL STUDIES

In order to provide experimental data for comparison to the numerical predictions, a series of wind tunnel tests was carried out using IAR facilities. This section describes the experimental program, presents summaries of key results and then uses these results to predict the effect of roughness on aircraft stall speed. The discussion then turns to observed effects of roughness on the roll control of a wing with an aileron.

2.1 Description of Experiments

The IAR 2 m by 3 m Low Speed Wind Tunnel was used to test a simple wing-aileron model with and without roughness applied to the wing. The model was an unswept, reflection-plane wing with a span, b, of 1.18 m, a constant chord, c, of 0.46 m and an untwisted NACA 4415 airfoil section, Figure 1a. The model had been used previously in a study [1] with a nacelle and operational propeller, but without aileron deflection. For the present study, the nacelle and propeller were not installed, thus giving a wing of constant airfoil section over the full span and a reflected aspect ratio of 5.3. The aileron was a plain, hinged type of 30 percent chord. Taking y as the coordinate along the span of the wing, the aileron extended from $y/b = 0.41$ to $y/b = 0.88$, i.e., approximately 50 percent of the wing span. Five aileron deflections, δ, were studied: 0°, ±10° and ±20°, where positive aileron deflections are defined as trailing edge down, Figure 1a. The main balance of the wind tunnel measured the loads and moments on the wing. Chord-wise surface pressures on the wing and aileron were measured at $y/b = 0.63$ and $y/b = 0.81$. The standard corrections for wall interference [7] were applied to the coefficient data and to the angle of attack, α. The test Reynolds number and Mach number were 3×10^6 and 0.3, respectively.

Three-dimensional roughness was applied to the upper surface of the wing to simulate the roughness that could be expected from failed anti-icing fluid. The roughness was confined to the region of the wing directly upstream of the aileron (see Figures 1a and b). Uniformity of roughness height, k, and density, $1/D^2$, were maintained using templates during roughness application. The templates were pliable plastic sheets with randomly-distributed, laser-cut holes. When held tightly against the wing's surface, the templates provided a mask through which the roughness material (a polyester resin) was applied. The thickness of the plastic sheet material thereby set k once all of the uncured resin was

scraped off the sheet, leaving resin only in the laser-cut holes. Removal of the sheet after the resin had cured left the roughness elements adhering to the surface of the wing in the form of randomly-distributed cylinders (see Figure 2) each with a height-to-diameter ratio of one sixth. The roughness has been categorized [5, 8 and 9] in terms of its non-dimensional height, k/c, its density, $1/D^2$ (number of roughness elements per dm^2), and its non-dimensional spacing, λ, where $\lambda = D^2/A_F$ and A_F is the frontal area of a typical individual roughness element. Note that D^2 (i.e., the reciprocal of $1/D^2$) is thus the average "clear" area surrounding an individual roughness element and includes the surface area under the element itself. The parameter λ is thus seen to be the ratio of two areas and indicates the elemental spacing in relation to the size of the element. The roughness extended from the leading edge to various fractions of c as outlined in Table 1.

Table 1 Roughness geometric parameters

k/c	$1/D^2$ (per dm^2)	$\lambda = D^2/A_F$	Coverage to:
0.0005	775	46	0.3c
0.0005	775	46	0.15c
0.0005	775	46	0.02c
0.0003	775	130	0.15c
0.0006	155	140	0.15c

2.2 Discussion of Experimental Results

Figures 3 to 7 show plots of the lift coefficient, C_L, versus α for each aileron deflection. In each figure, the results labeled "Clean" are for the wing without roughness. Considering only the curves for the clean wing, it is clear that as δ was varied, the qualitative changes in C_L at $\alpha = 0°$ and in maximum lift coefficient, C_{Lmax}, were as expected. There is some lack of precision in the angle of attack at stall, α_S, and in C_{Lmax}, resulting from the choice of 2° for the experimental increment in α.

The stall behaviour of the clean wing is considered first, before the effects of roughness are discussed. The surface pressure distributions showed that the clean wing generally exhibited a trailing-edge stall, wherein the flow separation on the upper surface began at the trailing edge and progressed steadily toward the leading edge as α increased. A trailing edge stall usually manifests itself in the shape of the C_L, versus α curve by exhibiting a gentle (as opposed to steep) negative slope in the curve after C_{Lmax} is reached (for example, see Figure 3). However the wing with $\delta = 20°$ (see Figure 5) was

somewhat of an exception to this behaviour. It exhibited the steepest, post-stall reduction in C_L and an inability to maintain a constant C_L for $\alpha > \alpha_S$. The wing with $\delta = 10°$ (see Figure 4) was a transitional geometry: its post-stall reduction in C_L was not as steep as the wing with $\delta = 20°$, but it was steeper than the other three aileron deflections. In addition, the surface pressure distributions showed that the flow on the upper surface of the aileron was separated for $\alpha \geq 8.5°$ when $\delta = 10°$; however, when $\delta = 20°$, the flow was separated for $\alpha \geq 0°$.

Generally, the addition of roughness did not alter the wing's tendency to exhibit a trailing-edge stall. As expected, α_S with roughness was lower than the respective clean case; however, in the post-stall region, the wing maintained a constant C_L (or a small negative slope for C_L versus α) for all roughness cases. The wing with $\delta = 20°$ (see Figure 5) was again somewhat of an exception to this, showing the steepest, post-stall reductions in C_L, measured from the maximum lift with roughness and for all roughness cases.

Keeping in mind the limitations imposed by the increments in α, Figure 8 shows that roughness with $k/c = 0.0005$ to $0.3c$ and $0.15c$ generally caused the greatest reductions in α_S (ranging from 4° to 6° reduction). When the coverage of this roughness was reduced to $0.02c$, α_S increased for a given δ and this response is consistent with a trailing-edge stall. As a result, the roughness with $k/c = 0.0005$ to $0.02c$ caused reductions in α_S of 4° for $\delta = 10°$ and 20° and only 2° for $\delta = 0°$, -10° and -20°. The other two roughness types (both to $0.15c$) caused reductions in α_S that were also in the range of 2° to 4°. Of the five aileron deflections, $\delta = 20°$ was always associated with the largest reductions in α_S for a given roughness type.

Consider now the effects of roughness on C_{Lmax}, being mindful that the experimental increment in α has again imposed a limitation on the precision of these reductions. Figure 9 shows that for a given δ, roughness with $k/c = 0.0005$ to $0.3c$ was generally associated with the largest percentage reductions in C_{Lmax} (ranging from 18 to 23 percent reduction), while roughness with $k/c = 0.0006$ to $0.15c$ was always associated with the smallest percentage reductions (ranging from 9 to 11 percent reduction). Furthermore, for all δ, roughness with $k/c = 0.0005$ to $0.15c$ consistently produced greater percentage reductions in C_{Lmax} than roughness with $k/c = 0.0006$ to $0.15c$. For this experimental study, the non-dimensional spacing, λ, for the roughness with $k/c = 0.0006$ was much greater than that for the roughness with $k/c = 0.0005$ (see Table 1). The greater spacing of the roughness elements for $k/c = 0.0006$ has reversed the trend in performance loss that is usually reported for roughness elements that have similar spacing [6]. For similarly spaced and shaped elements [9], the general trend is that increases in k/c lead to increased losses in C_{Lmax}. For this experimental study, generalizations regarding dependence on k/c alone for percentage reductions in C_{Lmax} are not sufficient. One must also include the non-dimensional spacing, λ, as an important descriptor for each roughness type.

For example, in a wind tunnel study of a proprietary two-dimensional airfoil in the IAR 2 m by 3 m Low Speed Wind Tunnel [10], λ was varied systematically. The roughness was created and applied to the model using the same method as in this present study and the resulting roughness cylinders also had a height-to-diameter ratio of one sixth. The

roughness coverage differed somewhat from the present study, extending from 0.15*c* on the lower surface to 0.05*c* on the upper surface. The Reynolds number and Mach number were similar to the present study at 2.7×10^6 and 0.26, respectively. It was found that for roughness with $k/c = 0.00025$, reductions in C_{Lmax} ranged from about 12 percent for $\lambda = 130$ to only about 1 percent for $\lambda = 1300$ (a variation in non-dimensional spacing by a factor of 10). For roughness with $k/c = 0.0005$, reductions in C_{Lmax} ranged from about 11 percent for $\lambda = 67$ to only about 3 percent for $\lambda = 330$ (a variation in non-dimensional spacing by a factor of 5). These results again show the powerful influence that roughness non-dimensional spacing has on reductions in C_{Lmax} for a given airfoil.

The survey of experimental studies by Lynch and Khodadoust [6] showed that, for a given airfoil-roughness combination, the reductions in C_{Lmax} generally increased with increasing Reynolds number. Thus, at higher Reynolds numbers than the present experimental value of 3×10^6, the percentage reductions in C_{Lmax} for this wing and aileron are expected to be greater than those reported here.

2.3 Effect of Roughness on Aircraft Stall Speed

The reductions in C_{Lmax} can also be used to indicate trends in the effects that roughness will have on the 1 *g* stall speeds of an aircraft equipped with a wing similar to the one studied here. For 1 *g* flight, when the clean wing reaches its stall speed, $V_{s\text{-}c}$, it is flying, by definition, at its clean $C_{Lmax\text{-}c}$ and the two are related through:

$$W = C_{L\max\text{-}c} \cdot \tfrac{1}{2} \cdot \rho \cdot V_{s\text{-}c}^2 \cdot S$$

where W is the weight of the aircraft, ρ is the air density and S is the wing reference area.

The 1 *g* stall speed relation is thus:

$$V_{s\text{-}c} = \sqrt{\frac{2 \cdot W}{\rho \cdot S \cdot C_{L\max\text{-}c}}} \tag{1}$$

Reductions in C_{Lmax} were previously quoted in percentages (see Figure 9), but for the remaining discussion these will be expressed in decimal fractions, R, where:

$$R = \frac{(C_{L\max\text{-}c} - C_{L\max\text{-}r})}{C_{L\max\text{-}c}}$$

and where $C_{Lmax\text{-}r}$ is the maximum lift obtained with a given roughness present. Re-arranging:

$$C_{L\max\text{-}r} = C_{L\max\text{-}c}(1 - R) \tag{2}$$

The stall speed for the wing with roughness is similarly expressed as:

$$V_{s\text{-}r} = \sqrt{\frac{2 \cdot W}{\rho \cdot S \cdot C_{L\max\text{-}r}}} \tag{3}$$

Substituting the expression for $C_{Lmax\text{-}r}$ from Equation 2 into Equation 3 gives:

$$V_{s-r} = \sqrt{\frac{2 \cdot W}{\rho \cdot S \cdot C_{L\max-c} \cdot (1-R)}}$$

which simplifies to:

$$V_{s-r} = \sqrt{\frac{1}{(1-R)}} \cdot V_{s-c} \tag{4}$$

Equation 4 can be applied with caution to the reductions in C_{Lmax} reported in Figure 9. Here, it is only appropriate to consider the aileron neutral setting, $\delta = 0°$. Transport aircraft rely on high lift devices to improve takeoff performance but the wing studied here did not incorporate such devices. Thus, these stall speed increases will be trend indicators only, not exact predictions for a full aircraft. Assuming that all of the aircraft's lift is produced by the wing, the selected reductions in C_{Lmax} produce the relative increases in stall speed shown in Table 2.

Table 2 Increase in stall speed due to roughness

k/c	Coverage to:	*R*, for $\delta = 0°$	$\frac{V_{s-r}}{V_{s-c}}$
0.0005	0.3*c*	0.216	1.130
0.0005	0.15*c*	0.185	1.108
0.0005	0.02*c*	0.145	1.081
0.0003	0.15*c*	0.104	1.057
0.0006	0.15*c*	0.107	1.058

Reference 11 points out that modern transport aircraft are required by certification to have a stall speed margin at takeoff of about 13 percent, meaning that the aircraft's safe takeoff speed must be 1.13 times higher than its 1 *g* stall speed for the clean wing takeoff condition. For the study of reference 12, the lift-off speed was chosen to give a 20 percent stall speed margin. Finally, reference 13 provides a table of lift-off speed safety margins that specifies 10 percent for FAA FAR Part 25 Transport Aircraft. From these references, one could conclude that the stall speed safety margin can be as low as 10 percent, with more conservative values being 13 percent and 20 percent.

Table 2 provides an indication that, if this wing was contaminated with roughness having *k/c* = 0.0005 to 0.3*c*, all of its stall speed margin could be eliminated if this margin was set at 13 percent. In other words, this wing could be dangerously close to stalling if the aircraft attempted to takeoff at its normal safe takeoff speed. A similar conclusion would

be reached for the combination of roughness having $k/c = 0.0005$ to $0.15c$ and a stall speed margin set at 10 percent.

2.4 Effect of Roughness on Pressure Distribution and Roll Control

Figures 10 and 11 show pressure distributions at the $y/b = 0.63$ station for two aileron deflections, 0 and 20°. In each figure the pressure distribution is for approximately $\alpha = 18.6°$ and each figure compares the clean wing case with that for $k/c = 0.0005$ to $0.3c$. The two cases with roughness exhibit an extensive region of separated flow on the upper surface, indicated by the flat pressure distribution from $0.2c$ to the trailing edge. As mentioned in the discussion of the wing's stall progression, Section 2.2, Figure 11 shows that, even for the clean wing with $\delta = 20°$, the flow on the upper surface of the aileron was separated for $\alpha < \alpha_S$. Thus the reduction in C_{Lmax} for $\delta = 20°$ arises mainly out of the roughness-induced flow separation on the upper surface of the wing *ahead* of the aileron only.

For good roll control authority [14], substantial changes in rolling moment, ΔC_l, are required with changes in δ. For two values of α, curves of ΔC_l versus δ are compared in Figure 12 for the clean wing and for the wing contaminated with $k/c = 0.0005$ to $0.3c$. Figure 12 re-states what was shown in Figures 3 to 8, that is, the wing with this roughness exhibited a lower α_S which is seen from a comparison of the two curves for nominally $\alpha = 16.5°$. In the rough condition and with a stalled wing at $\alpha = 16.5°$, the aileron provided marginal ΔC_l for a given δ compared to the un-stalled, clean wing at the same α. Clearly, at high angles of attack, the roll-control authority of the wing was severely compromised by the presence of this roughness.

Note that for the 1.83 m chord LS(1)-0417 airfoil of the experimental study reported in [2] and discussed below in Section 3, $k/c = 0.0005$ would correspond to a dimensional roughness height of only 0.9 mm. This is consistent with actual slush height estimates reported in [19].

3. NUMERICAL STUDIES

Both two and three-dimensional numerical analyses were carried out to study the effect of leading edge surface roughness on a wing with a deflected aileron. The three-dimensional numerical study relied on interactive boundary layer theory through the coupling of an inviscid potential and a boundary layer solution. The analysis of the wing with this tool provided information on the effects of the roughness in the linear portion of the lift curve. To better understand the flow near the maximum lift, a two-dimensional Navier-Stokes study was carried out. These simulations captured the trailing edge stall and provided insight into the loss of maximum attainable lift in a two-dimensional sense.

3.1 Two-Dimensional Navier-Stokes Analysis

The two dimensional (2-D) viscous analyses were carried out using the structured multi-block Navier-Stokes CFD solver, NPARC [15]. NPARC was developed under an alliance between the NASA Glenn Research Center and the Arnold Engineering Development

Center of the Department of Defense. It is a robust code that solves the governing equations using a Beam and Warming approximate factorization algorithm. It offers a variety of boundary conditions and turbulence models. For the current studies, the two-equation k-ω model by Wilcox was used without wall functions as it allows the specification of a surface roughness through the wall boundary condition applied to the specific dissipation rate ω [16]. A calibration study was carried out which determined the relationship between a given surface roughness and the equivalent sand grain roughness required by the model as implemented in NPARC.

The airfoil simulations were done on a single block C-mesh with 396 points defining the airfoil surface. The farfield was set at a distance of 20 chords and the freestream conditions were set to those of the experimental wing study described above. Maximum y^+ values of 0.2 were seen at angles of attack near stall.

3.1.1 Discussion of Two-Dimensional Navier-Stokes Results

The two-dimensional NS solver was applied to the NACA 4415 airfoil section with a 30 percent-of-chord aileron as defined by the experimental setup. The same five aileron deflections, as used in the wind tunnel experiment, were considered (0°, ±10° and ±20°). The surface condition of the airfoil was taken to be clean or roughened with elements equivalent to the k/c = 0.0005 experimental roughness. When roughened, three different extents of roughness (to 0.3c, 0.15c and 0.02c) were simulated for that one roughness type.

The effect of aileron deflection on the lift coefficient of the clean NACA 4415 airfoil section is shown in Figure 13. The maximum lift coefficient attainable by the airfoil increases as the aileron is deflected downwards but this increase is accompanied by a reduction in α_S. It can also be noted from this figure that modifying the camber of the airfoil with aileron deflection changes the rate at which the C_L, versus α curve approaches stall with the downward deflections having a more gradual roll-off of the curve. Finally, the maximum positive deflected aileron ($\delta = 20°$) shows a decrease in slope of the curve indicating that flow features other than a progressive trailing edge separation are present.

Figure 14 presents the effect of adding roughness to the NACA 4415 airfoil section. This figure shows that the roughness, as expected, decreases the maximum attainable lift and reduces the angle at which that lift is attained. The reduction in maximum attainable lift (Figure 15) for this airfoil without the aileron deflected is proportional to how much of the upper surface of the airfoil is covered with roughness. Nevertheless, small extents of roughness ahead of the suction peak can cause a significant loss of maximum lift. With the aileron deflected (Figure 16), the percentage loss in maximum lift is also a function of the deflection angle. Figures 15 and 16 include experimental data for illustrative purposes. Comparisons between experimental data and Navier-Stokes calculations should be done with caution as the former is a three-dimensional configuration having an aileron and roughness that are part-span and the latter is a two-dimensional geometry. The presented computed results indicate that the airfoil with an aileron deflected upward is more susceptible, in terms of percentage loss of lift, to leading edge roughness than with an aileron deflected downward.

3.2 Three-Dimensional Viscous Analysis

The numerical method is based on the interactive boundary layer theory, and involves interaction between inviscid potential and boundary layer solutions. A potential solution is obtained by using a panel method while the boundary layer solution is obtained by solving the three-dimensional (3-D) integral boundary layer equations [3 and 5]. This method has been demonstrated to be very efficient with little loss in accuracy for a broad range of applications. The effects of roughness are introduced into the boundary layer solution following the method due to Dvorak [17]. The numerical program is given the name PMAL3D, which stands for "Panel Method, Aerodynamics Laboratory, Three-Dimensional". It has been applied to a complete aircraft configuration, a flapped wing and to the wing-aileron combination described above.

3.2.1 Discussion of Three-Dimensional Viscous Results

Three different configurations have been studied and the results are analyzed and discussed. They are the Fokker F-28 MK1000 aircraft with aileron deflections, an NASA LS(1)-0417 wing-flap combination [2] and the NACA 4415 wing-aileron combination.

Fokker F-28 MK1000

The Fokker F-28 MK1000 without aileron deflection was previously investigated by Su and Crabbe [5]. Figure 17 shows the geometry of Fokker F-28 MK1000 aircraft and the surface paneling used in the current calculations. In total, 2564 panels were used for the whole configuration with 1364 panels covering the wing and flap. In this report, both whole and half configurations are studied. The paneling is symmetric about the centerline of the fuselage for the full aircraft. As before [5], the vertical fin and rudder are not included since their aerodynamic influence is negligible for a symmetric aircraft configuration under zero sideslip angle as investigated here.

The C_L, versus α curve for the Fokker F-28 without aileron deflection was calculated and is presented in Figure 18. The upstream flow speed of this earlier study was set at 70 m/s (136 knots) giving a Reynolds number based on the mean chord (3.51 m) of 17.5×10^6. Ground effect was not included, i.e., free air simulations were computed. It is shown that the potential solution obtained by PMAL3D is in very good agreement with PMARC (Panel Method, Ames Research Centre, a commercial panel method program) potential solution. With the three-dimensional boundary layer included, PMAL3D yields results close to the flight data with clean surfaces [18].

Since contamination during take-off is a major concern, the upstream flow speed was set to 57.8 m/s (112 knots, a typical take off speed) yielding a mean chord Reynolds number of 14.5×10^6. The flap was set at an 18° deflection. The aileron spans the outer 33 percent of span for 18 percent of chord from the trailing edge. For the Fokker F-28 half configuration, five aileron deflections (δ = -20°, -10°, 0°, 10°, 20°) were chosen. Since in normal flight operations, the ailerons on opposite sides of the aircraft are deflected in opposite directions, three cases of aileron deflections for the whole aircraft configuration were calculated, i.e., δ = 20° (-20°), δ = 10° (-10°), δ = 0° (0°). The positive down aileron deflection is on the starboard wing while the negative up aileron deflection is on the port wing.

The roughness case presented here has roughness covering the outer 30 percent of span for 0 to 30 percent of chord and covering the entire upper surface of the aileron. The roughness height was $k = 0.8$ mm and the non-dimensional spacing was $\lambda = 5.0$. This roughness case is referred to as "case 1".

Static tests conducted during the 1996/1997 winter [19] with a Fokker F-100, which has similar wing geometry to the F-28, showed that at the end of the Hold-Over Time (HOT) slush contamination of the Type IV fluid had an average height estimated at 0.65 mm and a peak height estimated at 0.85 mm with a density of 12 peaks/cm^2 (75 peaks/in^2). Other fluids may give rise to different roughness profiles. Almost all of the contamination occurred at the trailing edge with only minor points of contamination at the leading edge. This fluid failure pattern repeated over 13 tests and was independent of wind strength or direction, or precipitation type. Although the extent of leading edge contamination selected for study purposes would not occur in practice it was considered a valid reference condition for future studies.

Figure 19 shows the plot of C_L, versus α (potential solution) for the F-28 with various aileron deflections for both the half and whole configurations. The lift, C_L, was in linear relation with α. The aileron deflections also contributed linearly to the lift by the observation of uniform spacing between the individual curves of C_L, versus α for the half configuration. It was also observed that the increase in lift on one side of the aircraft (due to positive aileron deflection) compensated for the decrease in lift on the other side of the aircraft (due to negative aileron deflection), so that the resulting lift coefficient for the whole configuration was essentially the same for all aileron deflections.

The viscous results for the same configurations are presented in Figure 20. The maximum angle of attack that PMAL3D could handle was about 10° for $\delta = 0°$, -10°, -20° and about 8° for the downward aileron deflections $\delta = 10°$, 20°. While PMAL3D cannot deal with flow separations, the decrease in the maximum angle of attack that can be computed by PMAL3D for downward aileron deflections suggests that earlier separations may occur on the wing compared with the upward aileron deflections. This also was reflected in the calculations of the whole configuration with $\delta = 10°$ (-10°), 20° (-20°). It was again observed that for the whole configuration, the increase in lift on one side of the aircraft (due to positive aileron deflection) almost compensated for the decrease in lift on the other side of the aircraft (due to negative aileron deflection), so that the resulting lift coefficient for the whole configuration was essentially the same for all aileron deflections.

In Figure 21, the potential lift coefficients are compared with the clean viscous results for the half aircraft configuration. Note that the reduction in lift coefficient due to viscosity increases as the aileron deflection increases from $\delta = -20°$ to 20°. Increasing the downward aileron deflection induces more viscous effects on the lift coefficient and earlier separations. Comparison of the lift coefficient between the rough (case 1) and clean viscous solutions (see Figure 22) shows, due to contamination, the further reduction of lift coefficients for $\delta = 0°$, 10° and 20° and the further decrease of the maximum angle of attack computable by PMAL3D, indicating a possible reduction in the maximum lift coefficients. It was also observed that there was little change in lift coefficients for $\delta = -10°$ and -20° due to the contamination.

NASA LS(1)-0417 Wing-Flap

This configuration was used to perform wind tunnel experiments by IAR for investigating the aerodynamic effects of de- and anti-icing fluids that have been contaminated by varying quantities of freezing precipitation [2]. It was a rectangular wing and had a uniform NASA LS(1)-0417 airfoil section with a Fowler flap of 29 percent of chord. The span was 2.44 m. The flap was deployed at an angle of 15° corresponding to a typical setting for takeoff. The chord of the airfoil was 1.83 m with the flap retracted and 2.14 m with the flap deployed. The airfoil was mounted between end plates that were themselves mounted at a distance of 0.3 m from each side wall of the wind tunnel test section. The flow over the configuration was not two-dimensional because of a restriction on the size of these end plates. In order to capture the three-dimensionality of the resulting flow, the numerical calculations were carried out on an equivalent wing-flap configuration that had an aspect ratio of 15. The upstream flow speed was 40 m/s and the Reynolds number was 5×10^6 based on the chord of the airfoil with the flap retracted.

Plots of C_L, versus α for various conditions are given in Figure 23. PMAL3D yields quite reasonable potential results and clean viscous solutions that are in agreement with the experimental data. The numerical prediction for the contamination, covering the whole wing and exposed flap upper surface (flap directly under wing is not contaminated) with roughness height $k = 0.5$ mm and non-dimensional spacing $\lambda = 50$, is in good agreement with the experiment data with 10 minutes of snow contamination of a Type I de-icing fluid. The PMAL3D calculation for the case with roughness height $k = 1.0$ mm and non-dimensional spacing $\lambda = 10$, matches well with the experimental data with 17.5 minutes of snow contamination. Reference [2] reports that at 10 minutes of snow contamination, the snow falling onto the de-icing fluid was observed to melt shortly after impact, but by 17.5 minutes, the absorption capabilities of the fluid were exhausted and slush had accumulated rapidly on the wing. It should be noted that since there are no criteria or models known to the authors to derive the roughness parameters from the measurements of the contamination period, the parameters chosen here were only based on the authors' experience and observation.

NACA 4415 Wing-Aileron

This is the configuration tested in the IAR 2 m by 3 m Low Speed Wind Tunnel, as discussed in Section 2. In Figure 24, two-dimensional Navier-Stokes NPARC results are compared with PMAL3D clean viscous results. In order to achieve equivalent two-dimensional solutions, a rectangular wing with an aspect ratio of 60 was employed. Close agreement between the PMAL3D and NPARC results is another solid validation for the PMAL3D program.

Figures 25a to 25c present the comparison of C_L, versus α for the NACA 4415 wing with three different aileron deflections (0°, -10°, 10°). The results with roughness present are for the case with coverage to 30 percent of chord upstream of the aileron and with roughness height $k = 0.22$ mm ($k/c = 0.0005$) and non-dimensional spacing $\lambda = 46.1$. While the causes for the discrepancy between the PMAL3D predictions and the experimental data are not clear, the slope of the C_L, versus α curve and the roughness effects predicted by PMAL3D are in good agreement with the experiment carried out in

the 2 m by 3 m Low Speed Wind Tunnel. In an attempt to resolve the small discrepancy between the experimental and calculated C_L, versus α, the experimental and calculated pressure distributions were compared at two span-wise locations for three aileron deflections. Figures 26 to 28 show the comparison of the calculation for three aileron deflections with the corresponding experimental data. The overall agreement is good for the comparison of the upper surface pressure coefficients and the small discrepancy shown in the comparison of the lower surface pressure coefficients is consistent with the discrepancy shown in the curves of C_L, versus α.

4. CONCLUSIONS

Wind tunnel tests have been carried out to observe the effects of distributed roughness on the upper surface of a reflection-plane wing of aspect ratio 5.3 with a rectangular plan form, an NACA 4415 section and an aileron that occupied approximately the outer half of the wing span. The roughness extended from the leading edge to 2 percent, 15 percent or 30 percent of chord and the roughness was confined to the span-wise region of the wing upstream of the aileron only. Three types of roughness were investigated. The non-dimensional roughness height and spacing of each type were selected to simulate the roughness that may be encountered on a wing with failed anti-icing fluid upstream of the aileron.

The experiments showed that the presence of roughness always resulted in a reduction in the angle of attack at which the stall occurred. The largest reductions, which ranged from 4° to 6°, were created by the roughness with non-dimensional height, $k/c = 0.0005$, and spacing, $\lambda = 46$, covering 15 or 30 percent of chord. Nevertheless, when this roughness covered only 2 percent of chord, the stall angle was still reduced by 4° when the aileron was down and by 2° when the aileron was neutral or deflected up. Aileron down 20° was always associated with the largest reductions in stall angle of attack for each of the roughness heights and spacings tested, implying that if this wing were to be used on an operational aircraft, the wing with aileron fully down will stall before the wing with the up-going aileron.

Similar trends were observed in the experimental percentage reductions in maximum lift associated with each roughness type and extent. The roughness type with non-dimensional height, $k/c = 0.0005$, and spacing, $\lambda = 46$, covering 15 percent and 30 percent of chord, created the largest percentage reductions in maximum lift, ranging from approximately 17 to 23 percent reduction, depending on aileron deflection and extent of coverage. When this roughness covered only 2 percent of chord, the percentage reduction in maximum lift was between 12 percent and 15 percent, depending on aileron deflection. When the non-dimensional height was increased to $k/c = 0.0006$, but the non-dimensional spacing was increased to $\lambda = 140$ (with coverage to 15 percent of chord), the percentage reduction in maximum lift diminished to between 9 percent and 11 percent. Even though the non-dimensional height of the roughness had increased and the extent of roughness remained at 15 percent of chord, the greater spacing of individual roughness elements resulted in a diminished reduction in maximum lift, showing the importance of including the non-dimensional spacing of roughness elements when specifying roughness geometry.

Applying these experimental reductions in maximum lift to a hypothetical aircraft using this wing, it was possible to convert each reduction to an equivalent increase in the aircraft's 1 *g* stall speed. The roughness type with non-dimensional height, $k/c = 0.0005$, and spacing, $\lambda = 46$, covering 30 percent of chord, was found to be the most detrimental. It increased the stall speed by 13 percent, which is equal to the typical stall speed safety margin that is used to determine the takeoff speed for modern transport aircraft. In other words, this wing could be dangerously close to stalling if it attempted to takeoff at the specified normal takeoff speed. The same conclusion could be reached when this roughness type extended to only 15 percent of chord but with a stall speed safety margin of 10 percent.

The experiments showed that after the wing had entered the stall due to the presence of the roughness, the aileron provided marginal roll control compared to that just prior to the stall. Thus a roughness-induced premature stall on only one wing would be compounded by a loss of aileron effectiveness on that wing.

The two-dimensional viscous analyses of the NACA 4415 airfoil with an aileron were carried out using the structured multi-block Navier-Stokes solver NPARC. The two-equation k-ω model by Wilcox was used without wall functions as it allows the specification of a surface roughness. The following conclusions were drawn from the two-dimensional numerical analyses. The maximum lift attainable by the airfoil increases as the aileron is deflected downwards but is accompanied by a reduction in stall angle. The maximum positive deflected aileron shows a decrease in slope of the curve indicating that flow features other than a progressive trailing edge separation are present. The roughness, as expected, decreases the maximum attainable lift and reduces the angle at which that lift is attained. The reduction in maximum attainable lift for this airfoil without the aileron deflected is proportional to how much of the upper surface of the airfoil is covered with roughness. Nevertheless, small extents of roughness ahead of the suction peak can cause a significant loss of maximum lift. These two-dimensional observations are generally consistent with the above experimental analyses.

The Fokker F-28 MK1000 was investigated using PMAL3D and the computed results were compared with available flight data. A typical roughness case with aileron deflections was calculated. While PMAL3D cannot handle separations, the decrease in the maximum computable angle of attack by PMAL3D for downward aileron deflections may suggest that earlier separations occur on the wing compared with upward aileron deflections. The reduction in the maximum computable angle of attack by PMAL3D due to the presence of roughness may indicate a possible reduction in the maximum lift coefficient and the stall angle of attack.

For the NASA LS(1)-0417 configuration, the computed results from PMAL3D match well the experimental data with certain chosen roughness parameters. While this is a successful assessment for PMAL3D, it should be noted that since there are no criteria or models known to the authors to derive the roughness parameters from the measurements of the contamination period, the parameters chosen here were only based on the authors' experience and observation.

For the NACA 4415 configuration, PMAL3D yielded good agreement with the experiment in the slope of the lift curve and the aerodynamic effects of contamination. However,

there remains a discrepancy between the experiment and calculations across the whole linear portion of the lift curve, the causes of which are not clear.

Both experimental and numerical studies showed that roughness on an aircraft's wing at takeoff could have a negative impact on controllability. If a localized area of failed fluid goes undetected during the inspection prior to takeoff, its roughness could reduce the aircraft's roll-control at the completion of aircraft rotation when the angle of attack is increased to initiate the lift-off from the runway. Roughness will cause the wing to stall before it reaches the clean-wing stall angle of attack and a stall could occur if an attempt is made to rotate the aircraft very close to this angle of attack. In this scenario, it is expected that the undetected area of the roughness is small relative to the total wing area, but the roughness could be located on or near the leading edge, possibly on one wing only and ahead of an aileron. The extent of roughness coverage could be represented by the smallest studied here (2 percent of chord) resulting in a 2 to 4 degree reduction in stall angle of attack for the experimental NACA 4415 wing. If this roughness is present on only one wing during takeoff, and an attempt is made to rotate the aircraft to within a few degrees of its clean-wing stall angle of attack, the roughness could induce a localized premature flow separation leading to a significant loss of lift on the roughened wing. This study shows that along with a stalled wing there is a compounding problem of loss of aileron effectiveness, occurring at a time when normal roll control is required to correct the resulting un-commanded roll towards the compromised wing.

For an operational aircraft exposed to freezing precipitation on the ground, the larger extents of roughness coverage studied here (15 and 30 percent of chord), when translated into equivalent extents of failed fluid, should be large enough to be detected during the normal inspection prior to takeoff. Regulatory authorities require that all roughness be removed from the wing prior to takeoff. Even though the larger extents of roughness should be absent during takeoff, they were included in these studies to investigate the effect that changes in extent of coverage had on the magnitude of the aerodynamic penalties. These studies are expected to provide a reference for future work.

FIGURES

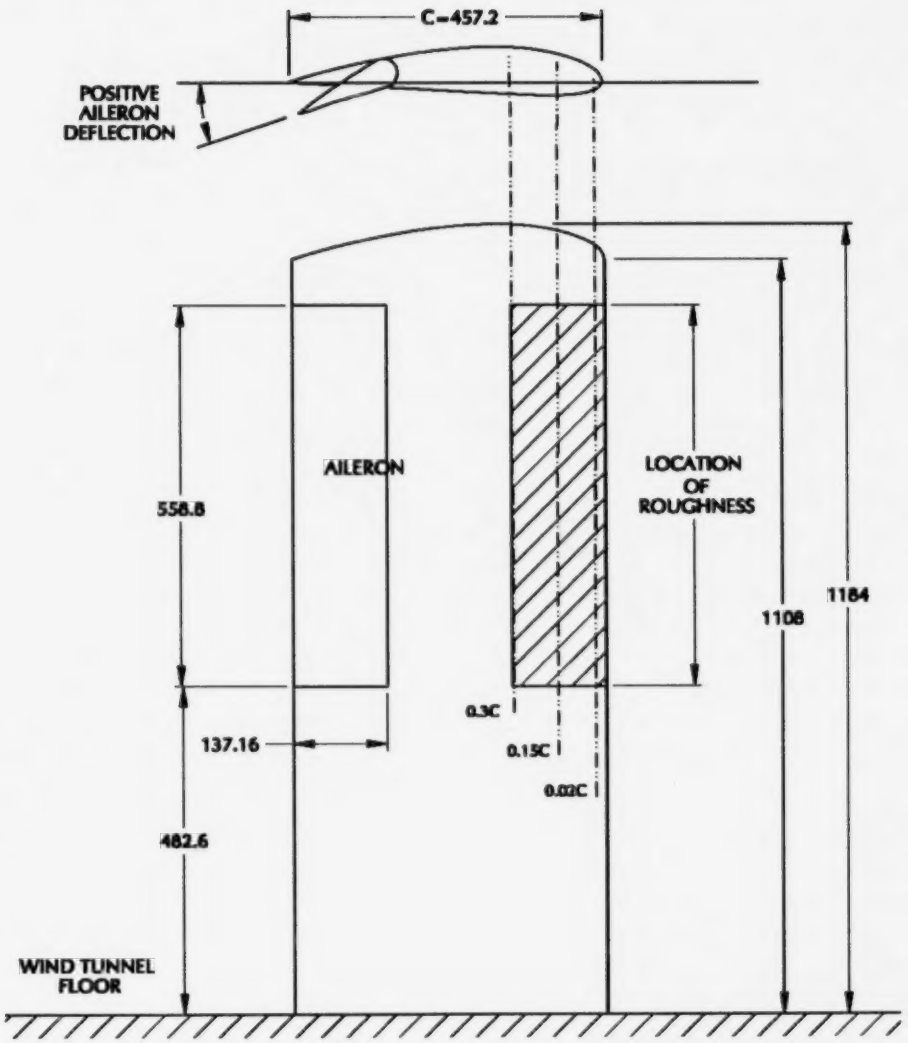

Figure 1a Wind tunnel model dimensions (mm)

Figure 1b Wind tunnel model with roughness to 0.02*c*; δ = -20°

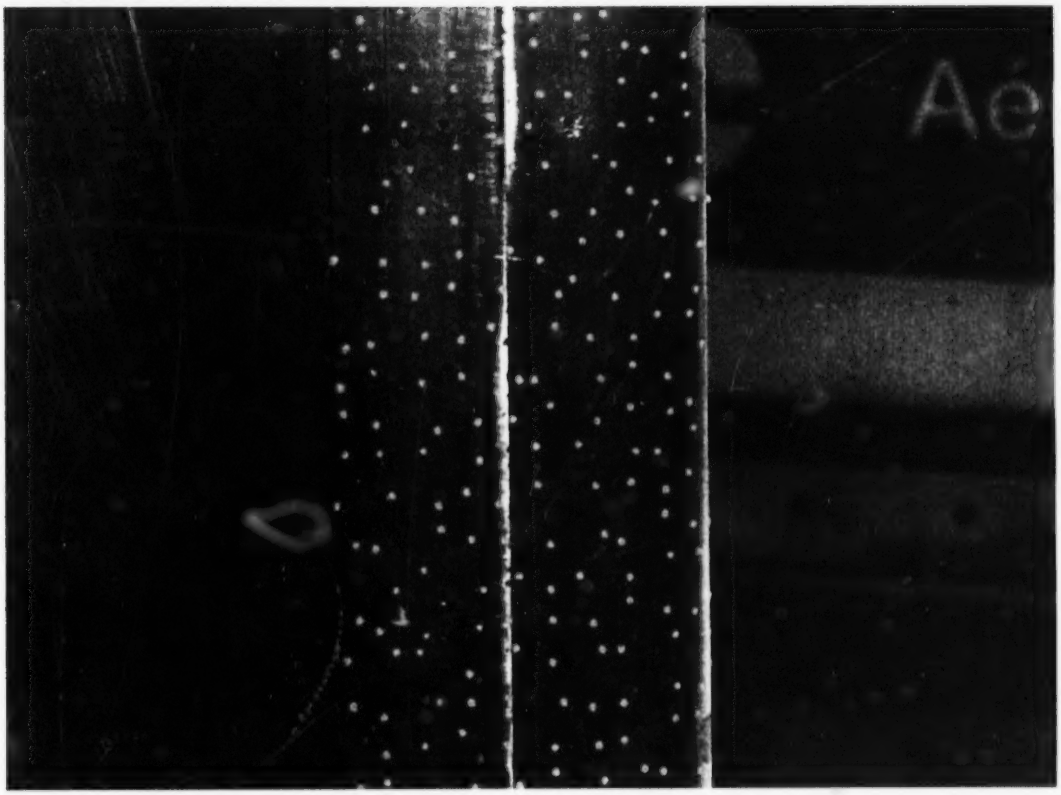

Figure 2 Roughness; $k/c = 0.0006$ to $0.15c$; $\lambda = 140$

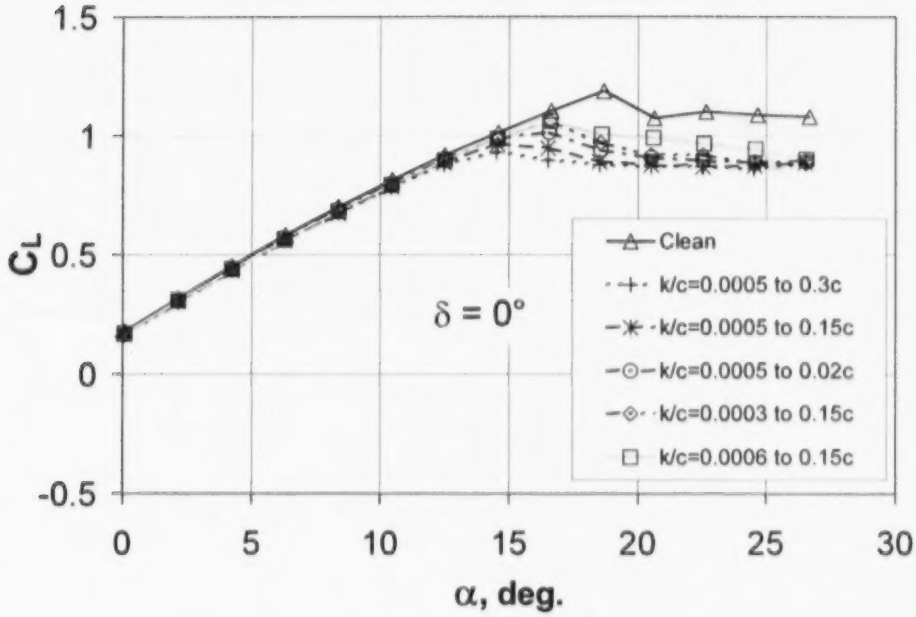

Figure 3 Experimental C_L vs. α; NACA 4415 wing-aileron; $\delta = 0°$

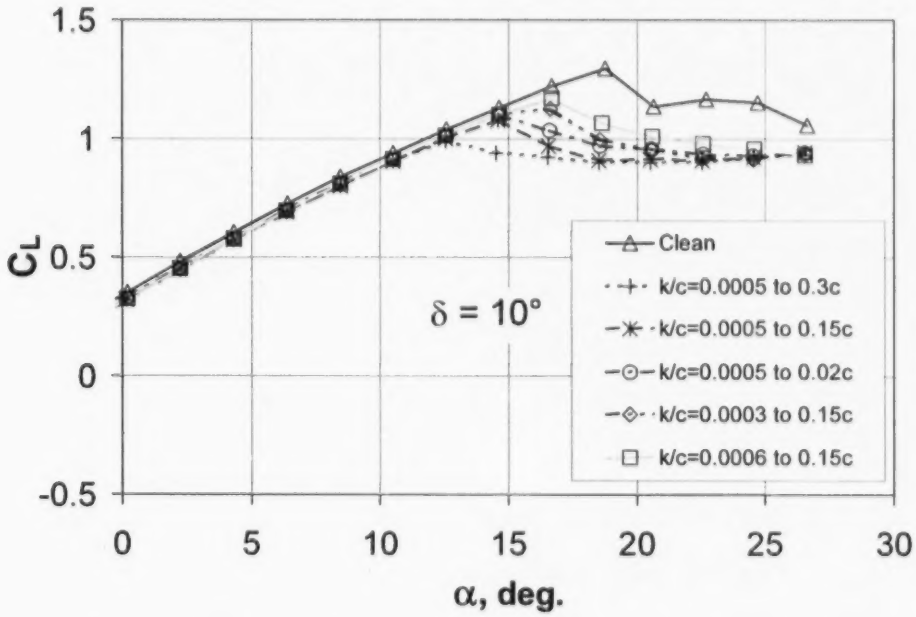

Figure 4 Experimental C_L vs. α; NACA 4415 wing-aileron; $\delta = 10°$

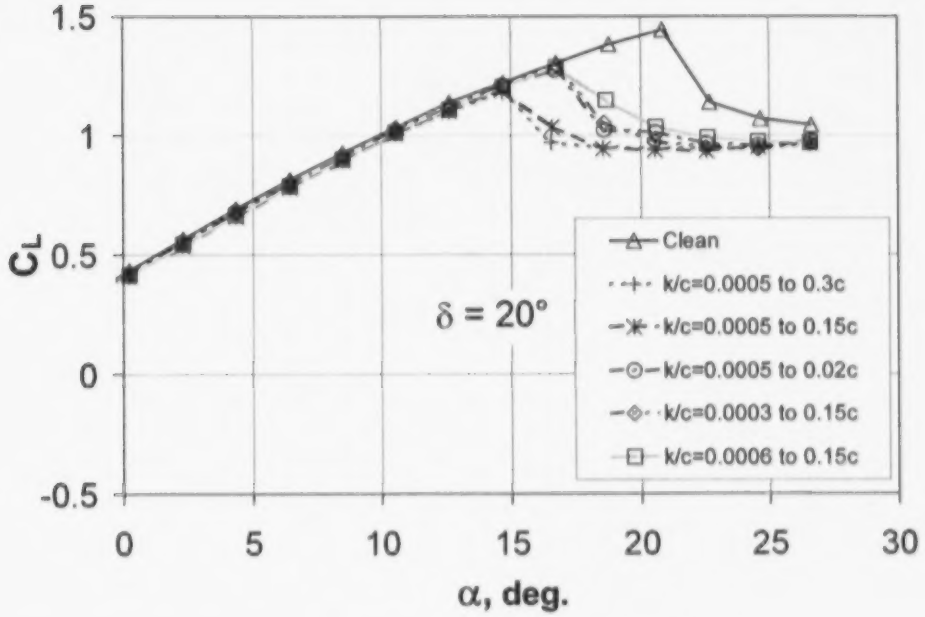

Figure 5 Experimental C_L vs. α; NACA 4415 wing-aileron; $\delta = 20°$

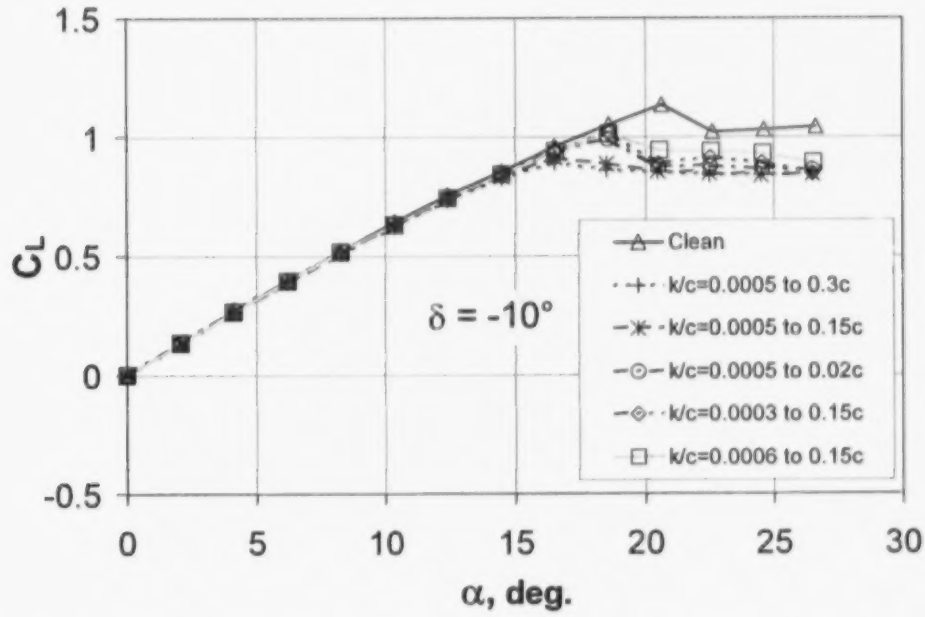

Figure 6 Experimental C_L vs. α; NACA 4415 wing-aileron; $\delta = -10°$

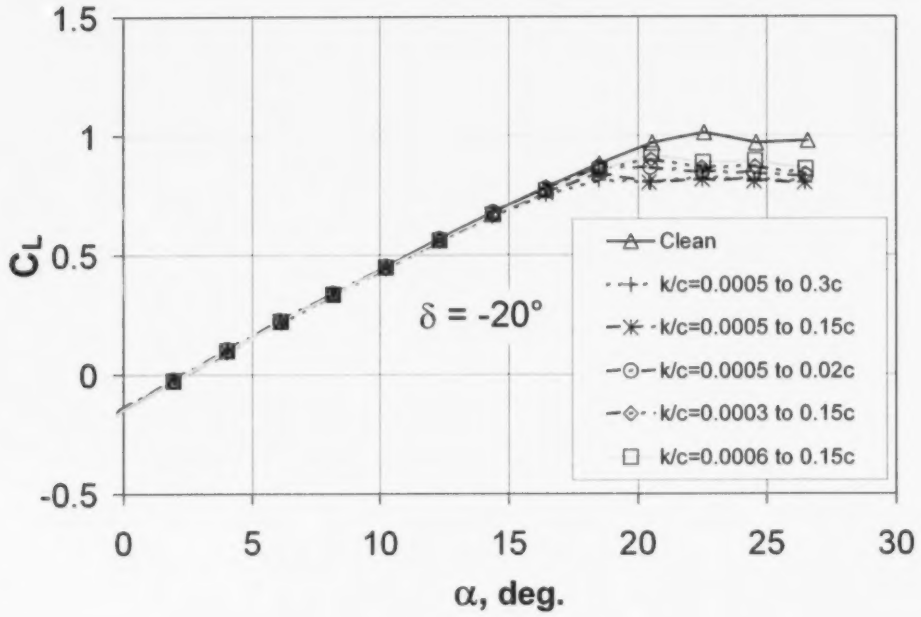

Figure 7 Experimental C_L vs. α; NACA 4415 wing-aileron; δ = -20°

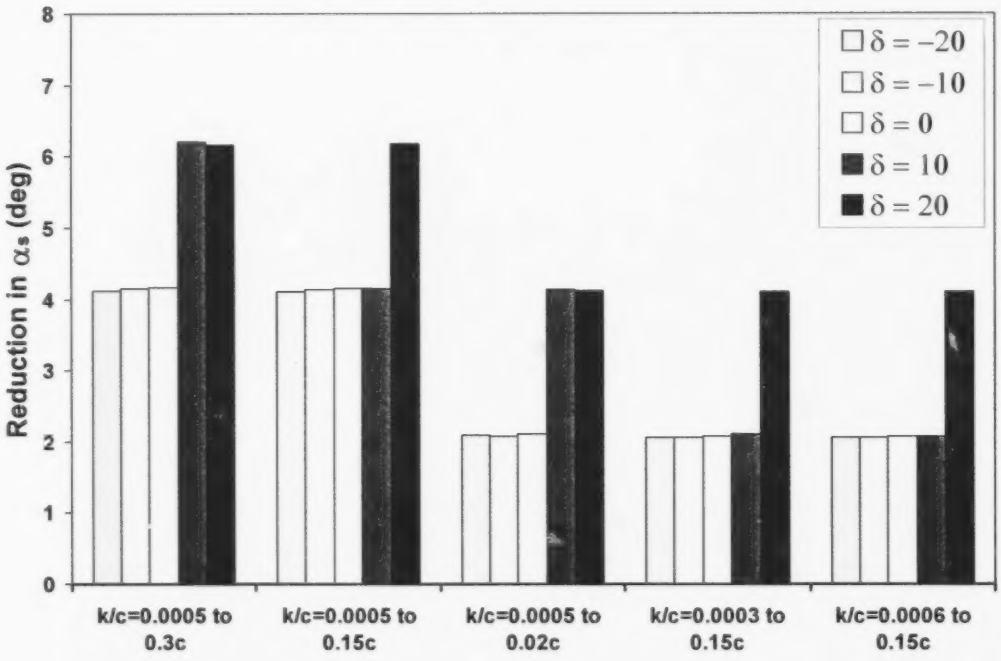

Figure 8 Experimental reduction in α_s

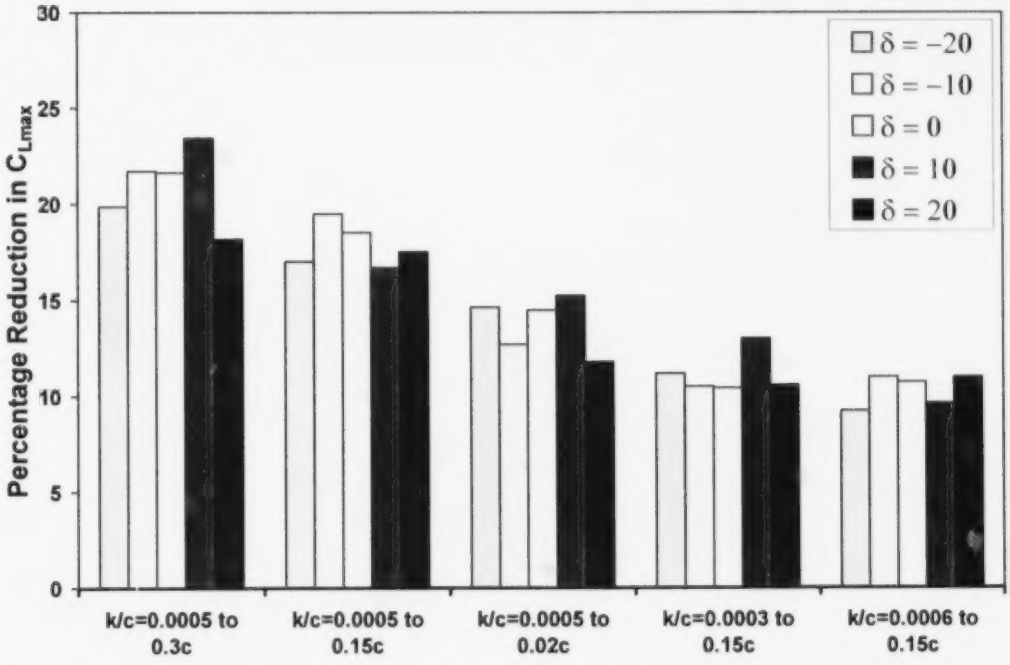

Figure 9 Experimental reduction in C_{Lmax}

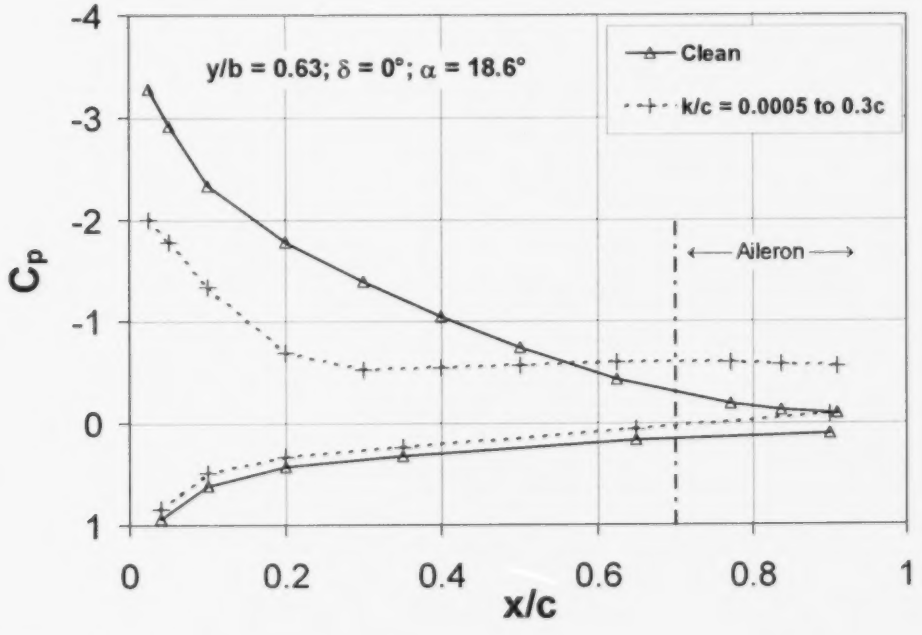

Figure 10 Experimental C_p vs. x/c; $\delta = 0°$

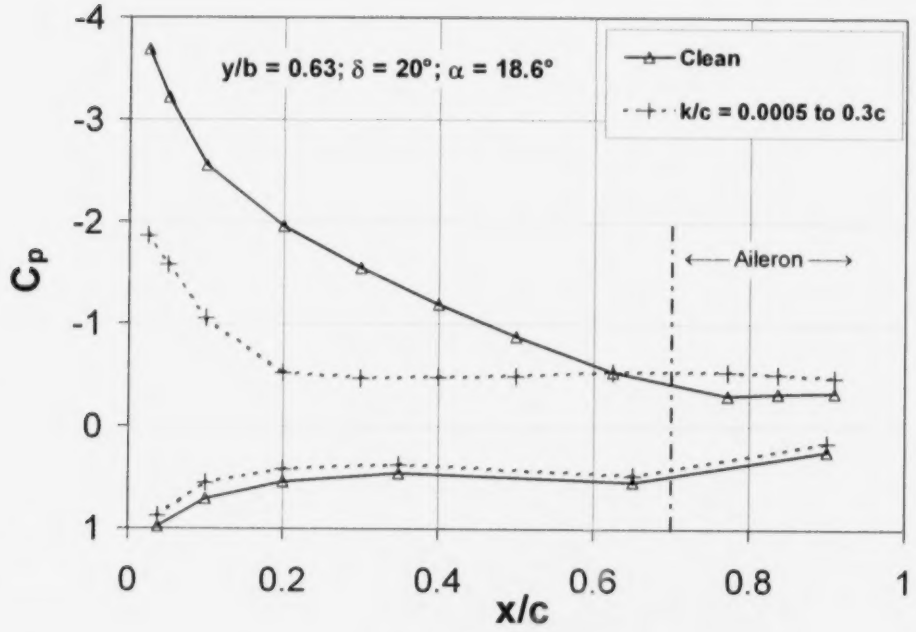

Figure 11 Experimental C_p vs. x/c; $\delta = 20°$

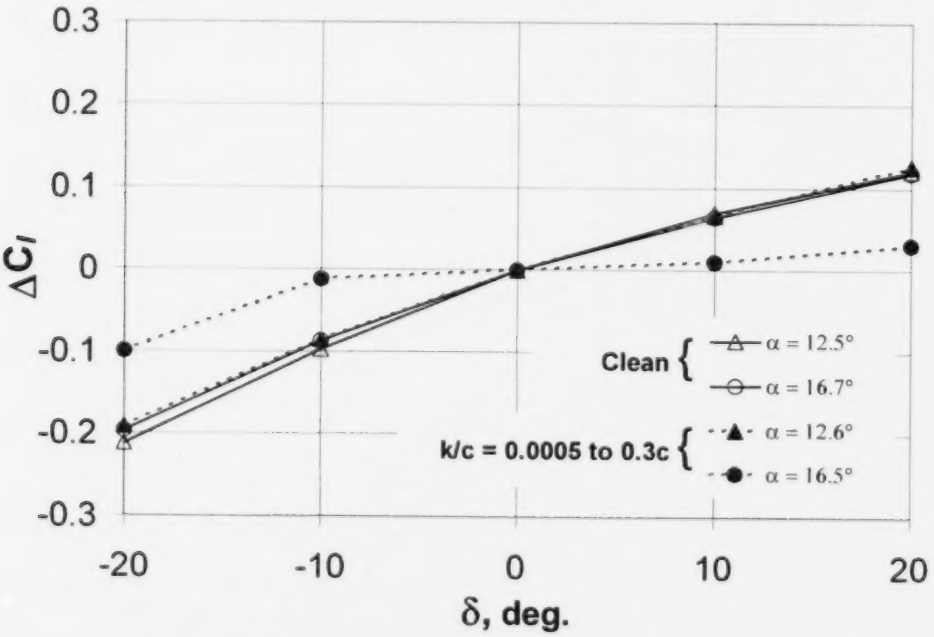

Figure 12 Experimental ΔC_l vs. δ

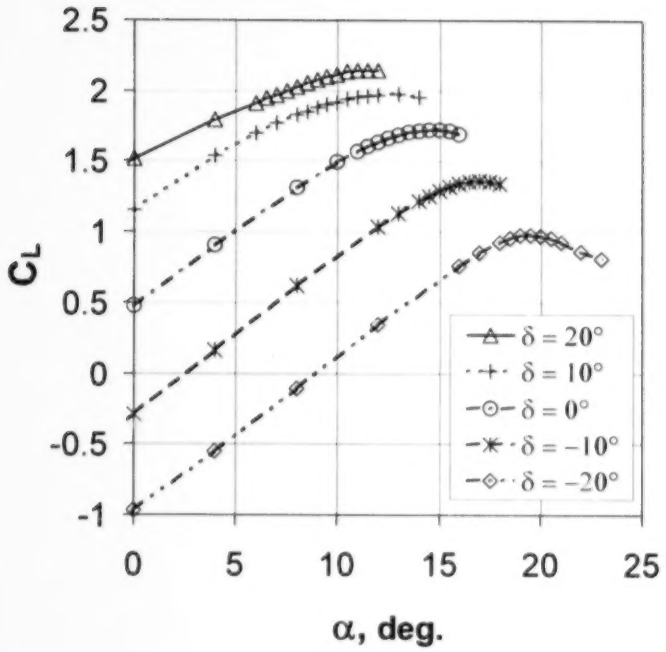

Figure 13 2-D NS C_L vs. α; NACA 4415 airfoil; clean surface

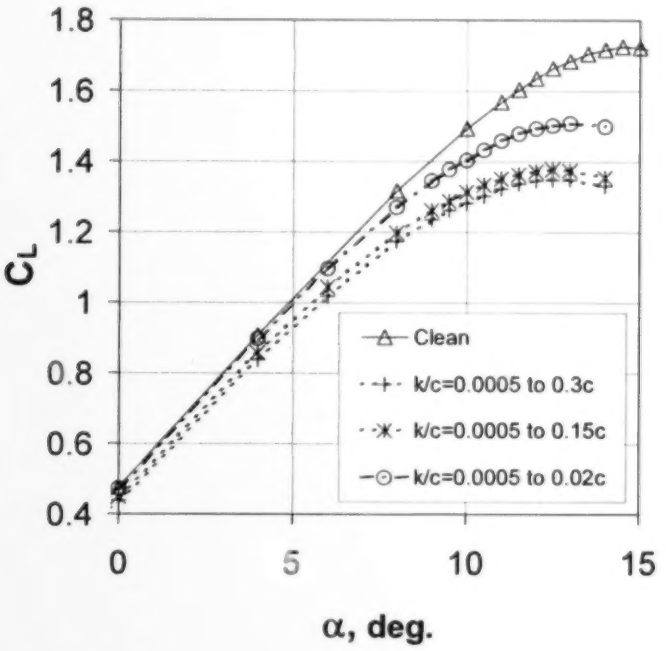

Figure 14 2-D NS C_L vs. α; NACA 4415 airfoil; $\delta = 0°$; clean and rough surface

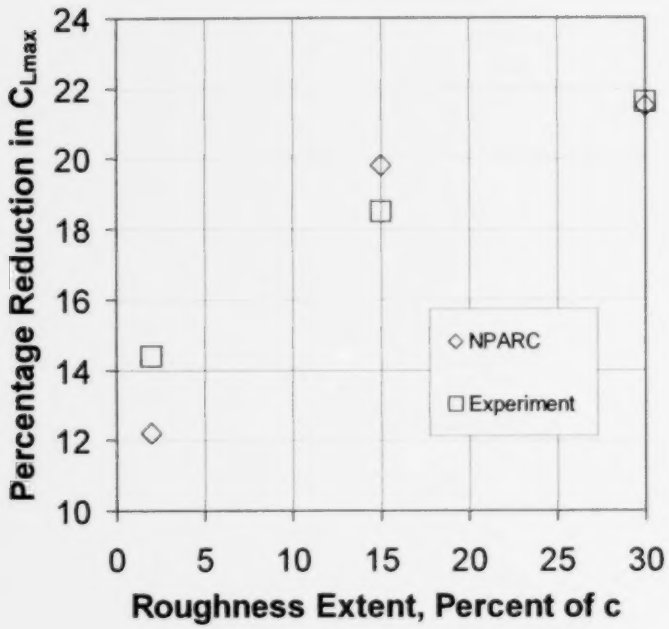

Figure 15 2-D NS reduction in C_{Lmax}; NACA 4415 airfoil; $\delta = 0°$

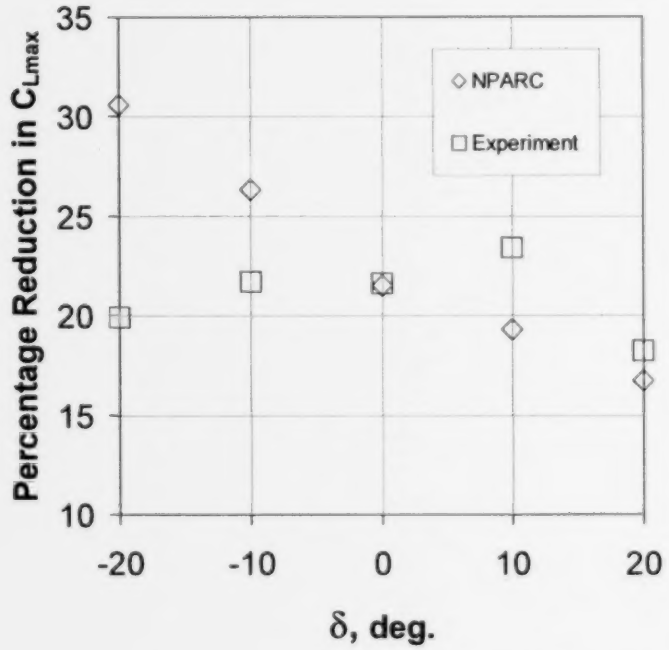

Figure 16 2-D NS reduction in C_{Lmax}; NACA 4415 airfoil; roughness to 0.3*c*

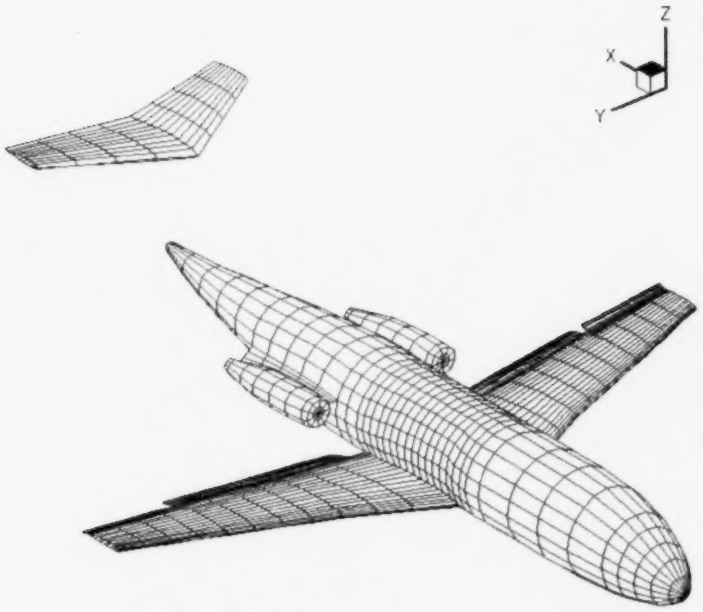

Figure 17 Surface paneling for Fokker F-28 MK1000 aircraft

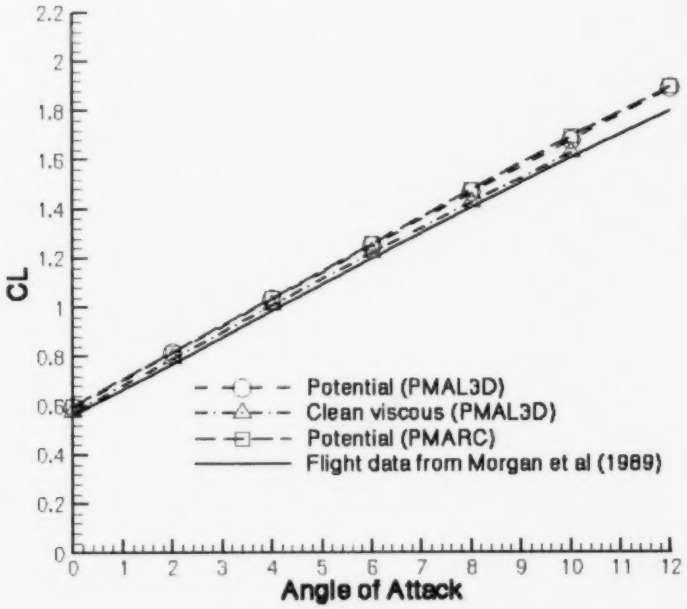

Figure 18 C_L vs. α; Fokker F-28; δ = 0°; 18° flap; Re = 17.5 x 10^6

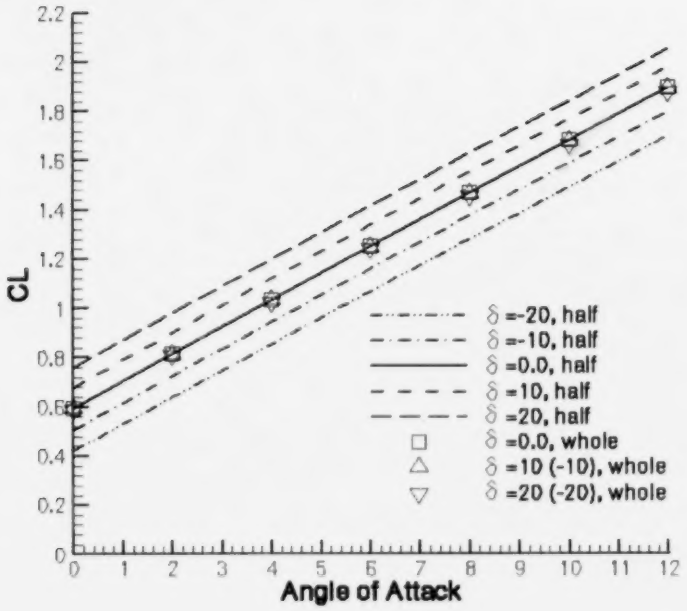

Figure 19 C_L vs. α; Fokker F-28; 18° flap; potential solution

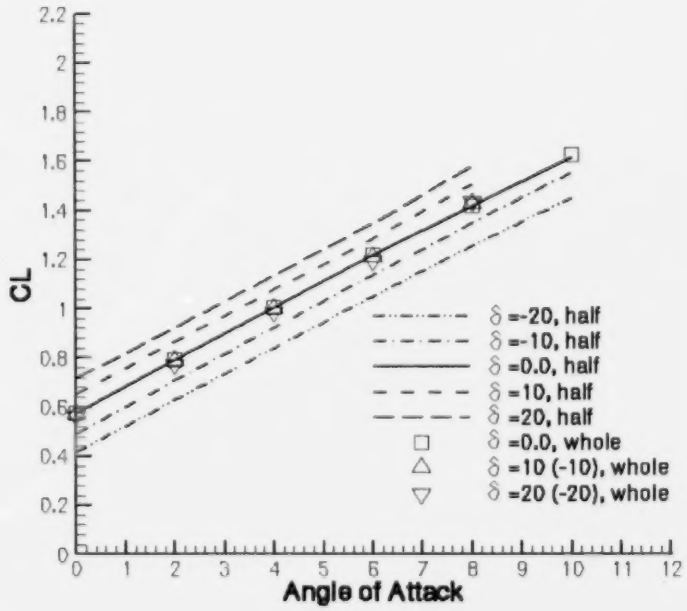

Figure 20 C_L vs. α; Fokker F-28; 18° flap; viscous solution; clean surface

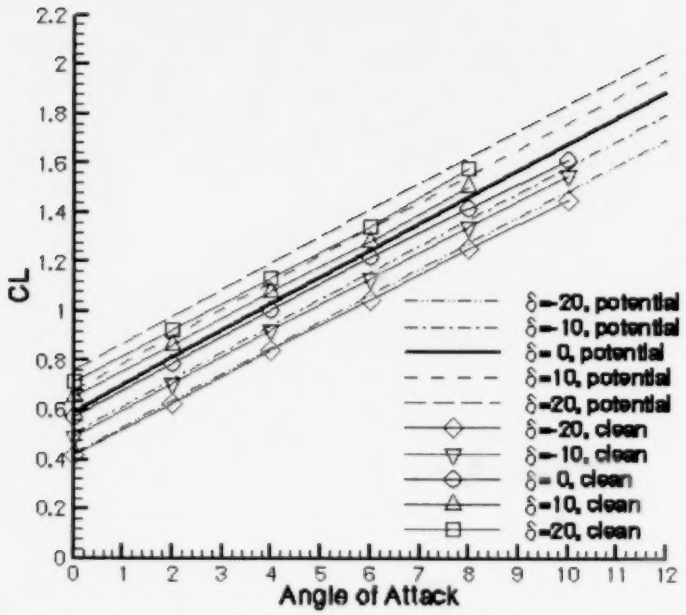

Figure 21 C_L vs. α; Fokker F-28; 18° flap; potential and viscous solutions

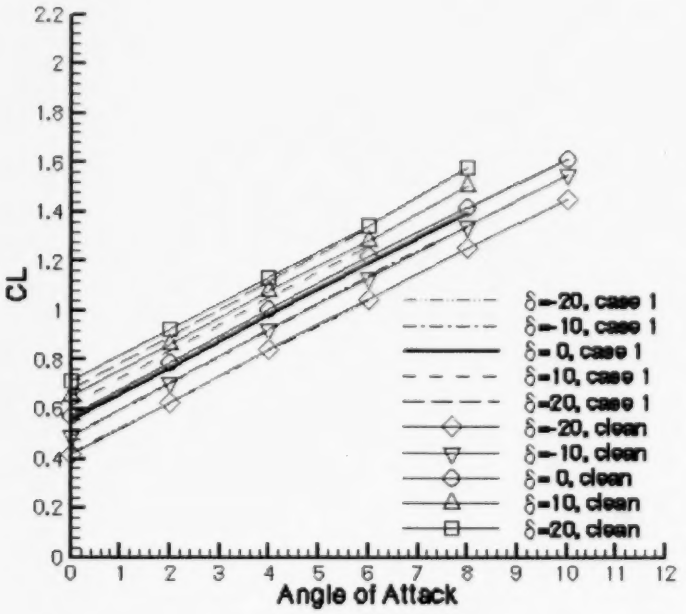

Figure 22 C_L vs. α; Fokker F-28; 18° flap; clean and rough viscous solutions

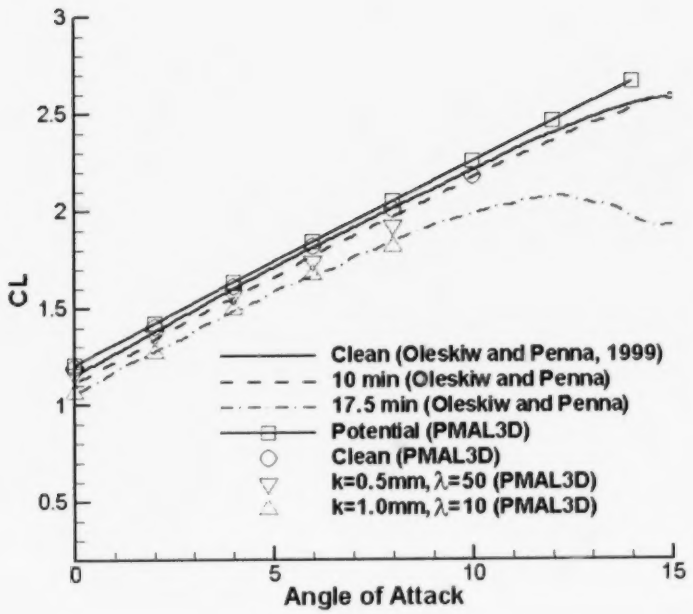

Figure 23 C_L vs. α; NASA LS(1)-0417 configuration; 15° flap; Re = 5 x 10^6

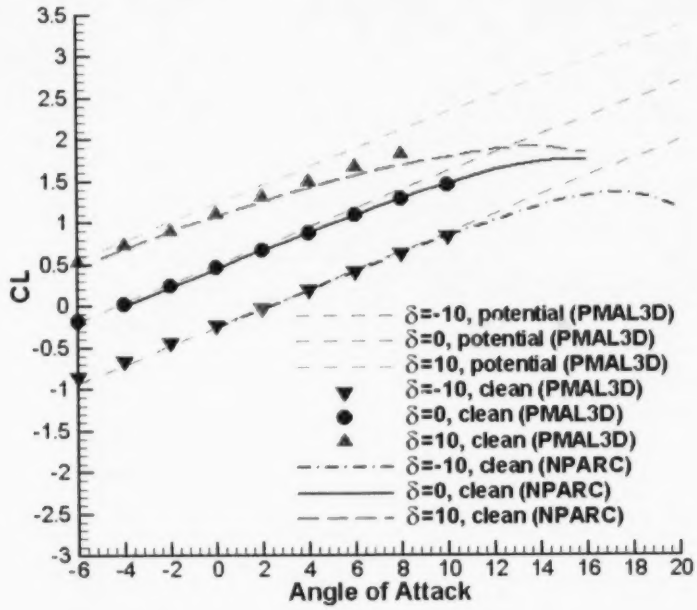

Figure 24 C_L vs. α; NACA 4415 airfoil; clean surface; Re = 3.2 x 10^6

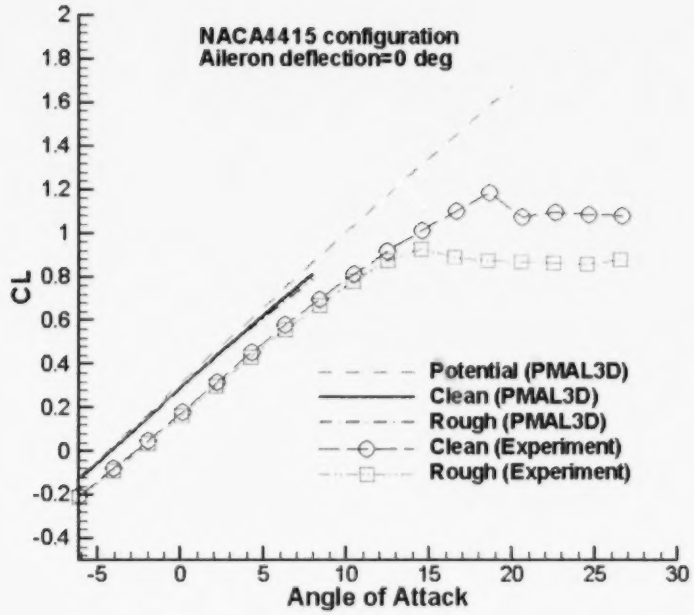

Figure 25a C_L vs. α; NACA 4415 wing; $\delta = 0°$; Re = 3.2 x 10^6

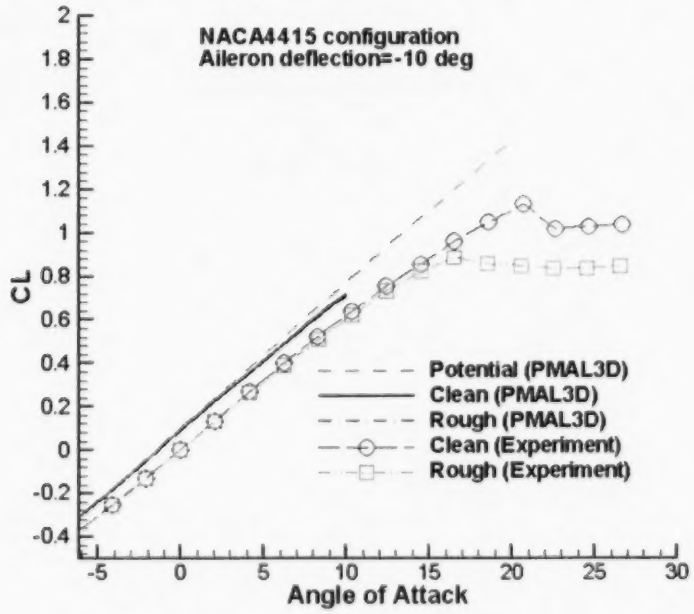

Figure 25b C_L vs. α; NACA 4415 wing; $\delta = -10°$; Re = 3.2 x 10^6

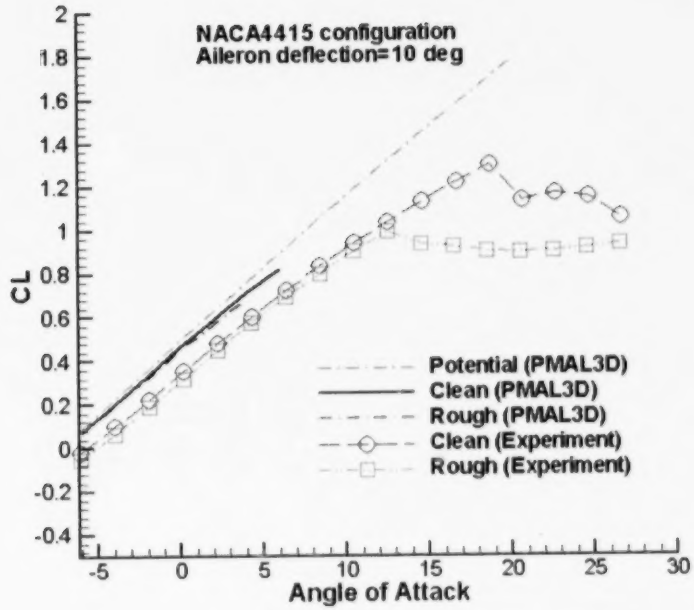

Figure 25c C_L vs. α; NACA 4415 wing; δ = 10°; Re = 3.2 x 10^6

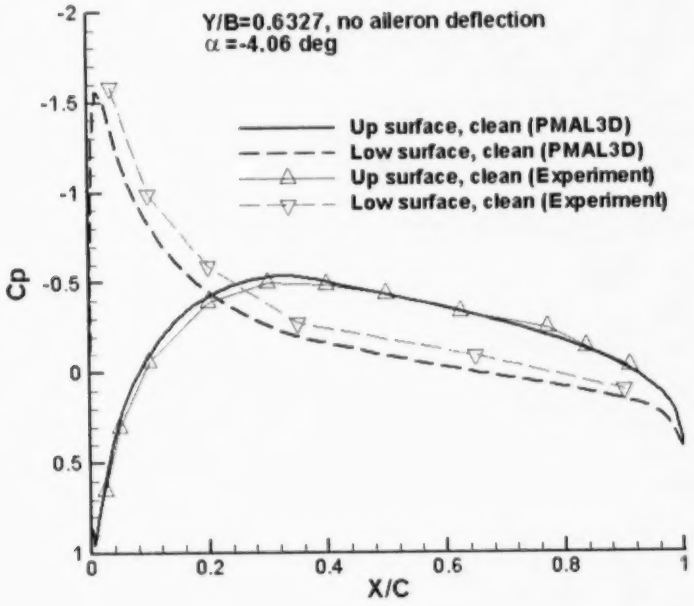

Figure 26a C_p vs. *x/c*; NACA 4415 wing; *y/b* = 0.63; δ = 0°; α = -4.06°

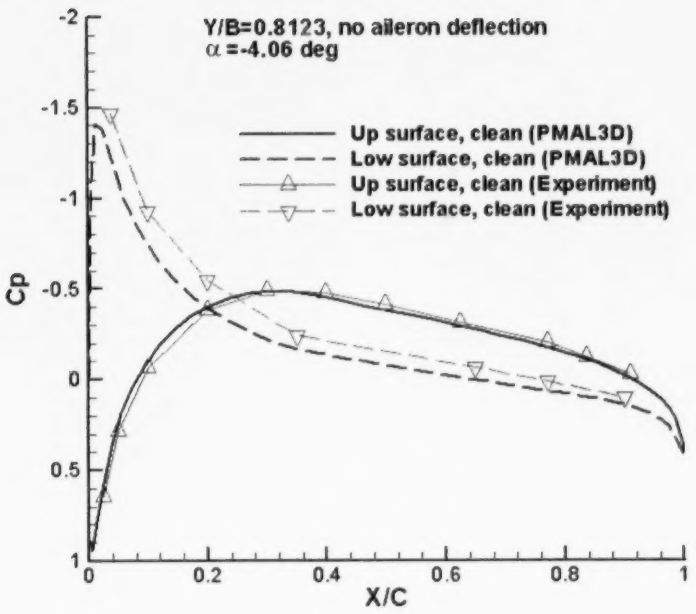

Figure 26b C_p vs. *x/c;* NACA 4415 wing; *y/b* = 0.81; δ = 0°; α = -4.06°

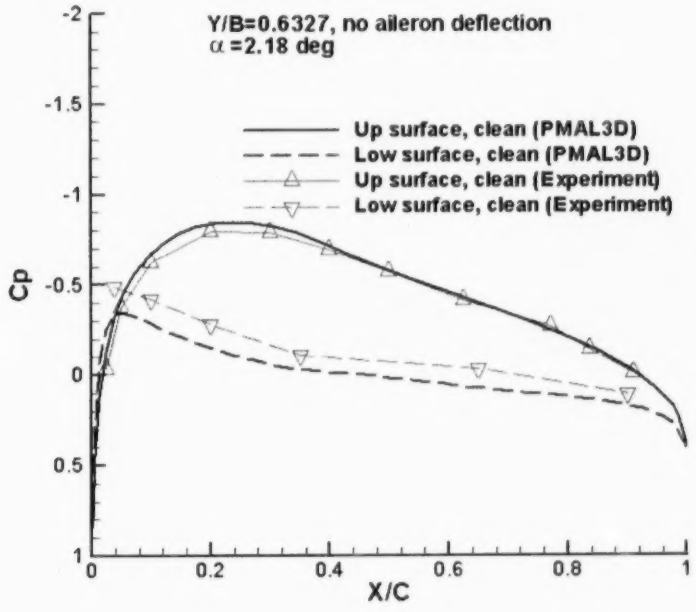

Figure 26c C_p vs. *x/c;* NACA 4415 wing; *y/b* = 0.63; δ = 0°; α = 2.18°

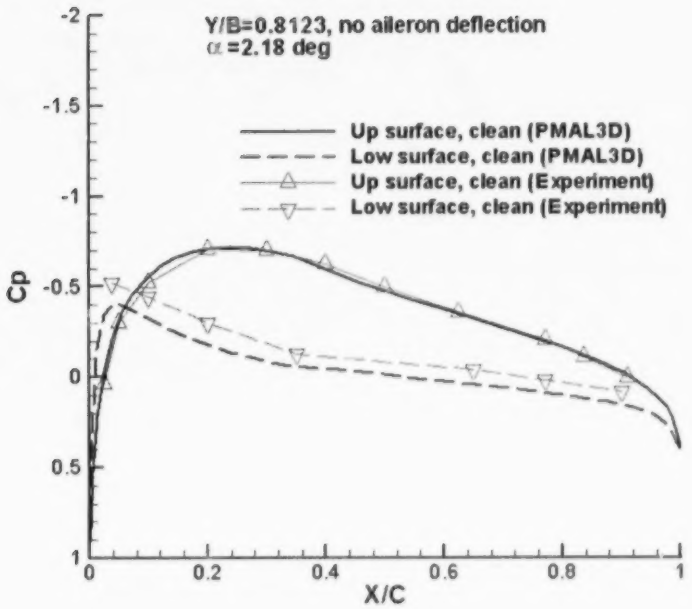

Figure 26d C_p vs. *x/c;* NACA 4415 wing; *y/b* = 0.81; δ = 0°; α = 2.18°

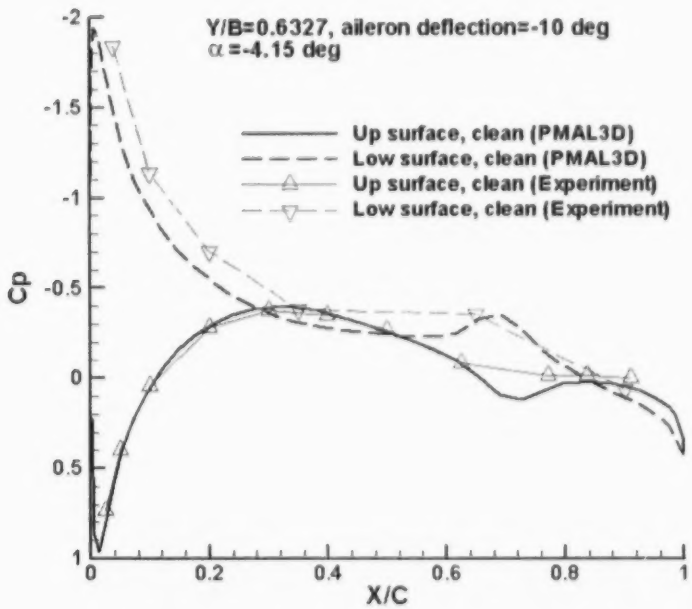

Figure 27a C_p vs. *x/c;* NACA 4415 wing; *y/b* = 0.63; δ = -10°; α = -4.15°

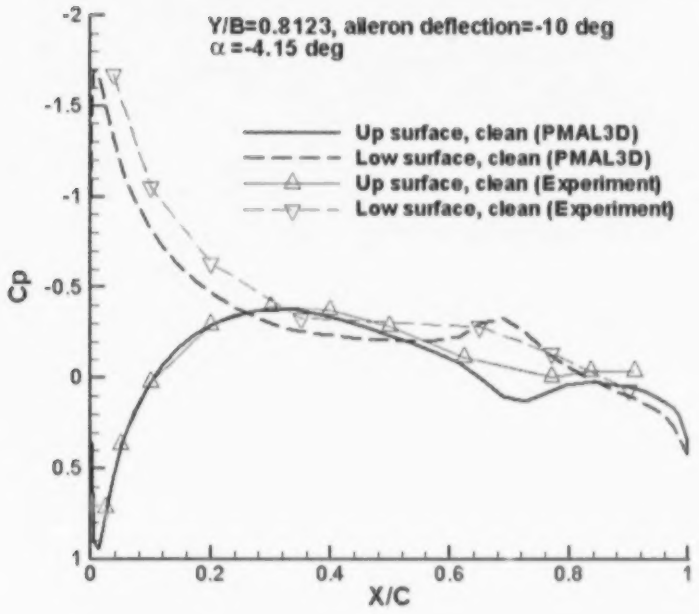

Figure 27b C_p vs. *x/c;* NACA 4415 wing; *y/b* = 0.81; δ = -10°; α = -4.15°

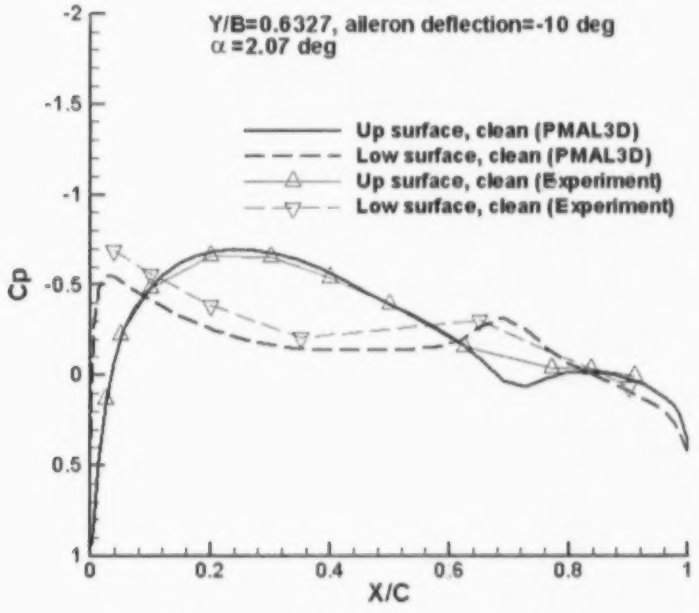

Figure 27c C_p vs. *x/c;* NACA 4415 wing; *y/b* = 0.63; δ = -10°; α = 2.07°

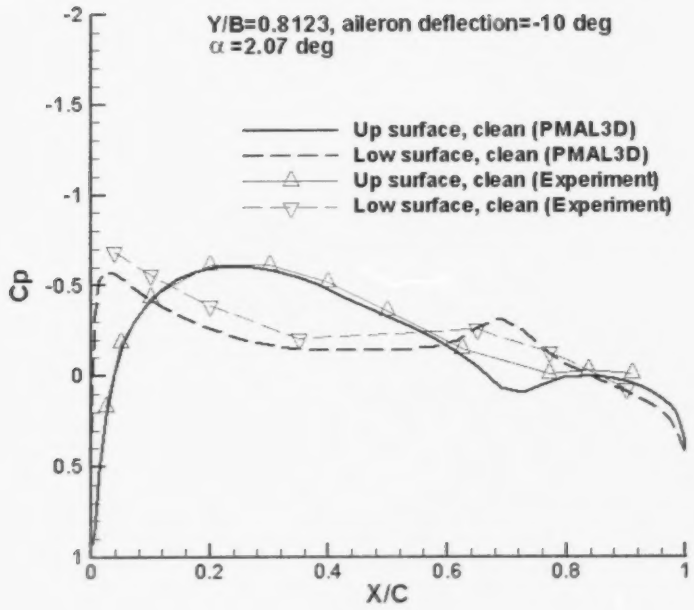

Figure 27d C_p vs. *x/c;* NACA 4415 wing; *y/b* = 0.81; δ = -10°; α = 2.07°

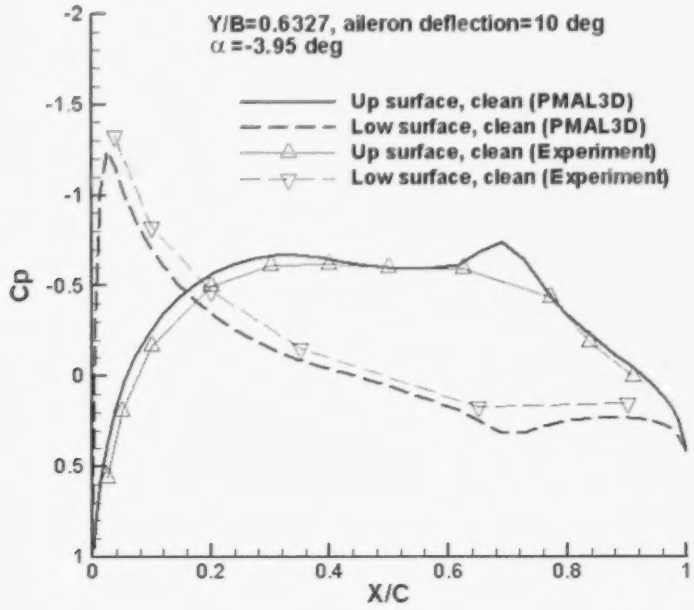

Figure 28a C_p vs. *x/c;* NACA 4415 wing; *y/b* = 0.63; δ = 10°; α = -3.95°

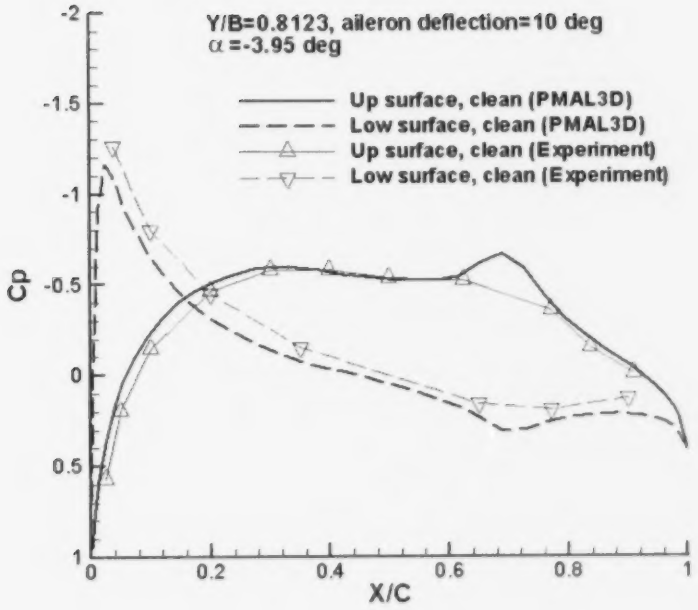

Figure 28b C_p vs. *x/c;* NACA 4415 wing; *y/b* = 0.81; δ = 10°; α = -3.95°

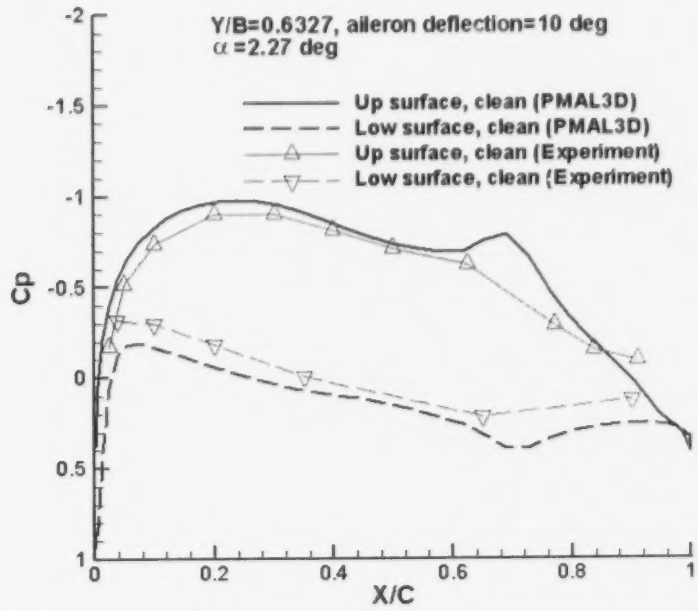

Figure 28c C_p vs. *x/c;* NACA 4415 wing; *y/b* = 0.63; δ = 10°; α = 2.27°

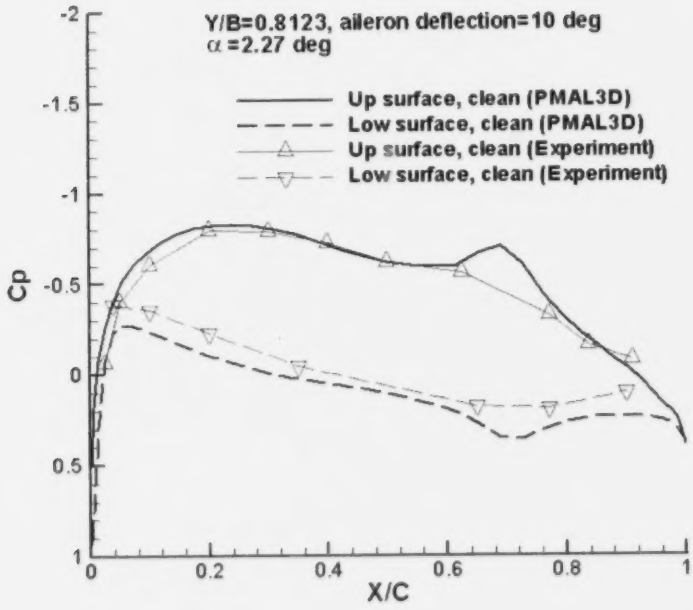

Figure 28d C_p vs. *x/c;* NACA 4415 wing; *y/b* = 0.81; δ = 10°; α = 2.27°

REFERENCES

1. Wickens, R.H. and Nguyen, V.D., "Wind Tunnel Investigation of a Wing-Propeller Model Performance Degradation due to Distributed Upper-Surface Roughness and Leading Edge Shape Modification", *Conference on Effects of Adverse Weather on Aerodynamics,* Advisory Group for Aerospace Research and Development, Toulouse, France, CP-496, Paper 11, 1991.

2. Oleskiw, M.M. and Penna, P.J., "Airfoil-Flap Performance with De/Anti-icing Fluids and Freezing Precipitation", Transport Canada, Transportation Development Centre, Montreal, Quebec, TP13426E, May 1999.

3. Crabbe, R.S., "Predicted Influence of Surface Roughness Including Fluid-runback Waves on Airfoil Lift and Drag", National Research Council Canada, Ottawa, Ontario, NRCC/IAR Laboratory Technical Report LTR-A-002, November 1995.

4. Oleskiw, M.M., Penna, P.J., Crabbe, R.S. and Byers, M.E., "Full-Scale Wind-Tunnel Simulation of Takeoff Performance Degradation with Contaminated Fluid Runback", Transport Canada, Transportation Development Centre, Montreal, Quebec, TP13925E, April 2002.

5. Su, J. and Crabbe, R.S., "Numerical Prediction of Aerodynamic Performance of a Complete Aircraft with Contaminated Wings and Flaps", *Proceedings of the 1998 American Society of Mechanical Engineers Fluids Engineering Division Summer Meeting*, Washington, D.C., June 21-25, 1998.

6. Lynch, F.T. and Khodadoust, A., "Effects of Ice Accretions on Aircraft Aerodynamics", *Progress in Aerospace Sciences,* Elsevier Science Ltd., Vol. 37, 2001, pp. 669-767.

7. Garner, H.C., Rogers, E.W.E., Acum, W.E.A. and Maskell, E.C., "Subsonic Wind Tunnel Wall Corrections", Advisory Group for Aerospace Research and Development, Neuilly-Sur-Seine, France, AGARDograph 109, October 1966.

8. Simpson, R.L., "A Generalized Correlation of Roughness Density Effects on the Turbulent Boundary Layer", *AIAA Journal,* American Institute of Aeronautics and Astronautics, Reston, Virginia, Vol. 11, No. 2, 1973, pp. 242-244.

9. Waigh, D.R. and Kind, R.J., "An Improved Correlation for the Aerodynamic Effects of Regularly-Spaced Three-Dimensional Surface Roughness Elements", *Aerodynamics Symposium of the 44th Annual Conference of the Canadian Aeronautics and Space Institute*, Toronto, Ontario, April 28-30, 1997, pp. 165-174.

10. Tezok, F. and Kafyeke, F., "Classification of Wing Leading Edge Roughness", *Aerodynamics Symposium of the 44th Annual Conference of the Canadian Aeronautics and Space Institute*, Toronto, Ontario, April 28-30, 1997, pp. 175-183.

11. Reinmann, J.J., "Icing: Accretion, Detection, Protection", *Lecture Series on Flight in an Adverse Environment*, Advisory Group for Aerospace Research and Development, Neuilly-Sur-Seine, France, LS-197, November 1994, Paper 4.

12. Kind, R.J. and Lawrysyn, M.A., "Performance Degradation due to Hoar Frost on Lifting Surfaces", *Canadian Aeronautics and Space Journal*, Ottawa, Ontario, Vol. 38, No. 2, June 1992, pp. 62-70.

13. Lan, C.E. and Roskam, J., *Airplane Aerodynamics and Performance*, Roskam Aviation and Engineering, Ottawa, Kansas, 1980, pp. 418-440.

14. Johnson, H.S. and Hagerman, J.R., "Wind-Tunnel Investigation at Low Speed of the Lateral Control Characteristics of an Unswept Untapered Semispan Wing of Aspect Ratio 3.13 Equipped with Various 25-Percent-Chord Plain Ailerons", National Advisory Committee for Aeronautics Technical Note TN-2199, October 1950.

15. "NPARC User's Guide", Published by the NPARC Alliance, Version 3.1, September 1996.

16. Yoder, D.A. and Georgiadis, N.J., "Implementation of a Two-Equation k-ω Turbulence Model in NPARC", American Institute of Aeronautics and Astronautics, Reston, Virginia, AIAA-96-0383, 1996.

17. Dvorak, F.A., "Calculation of Turbulent Boundary Layers on Rough Surfaces in Pressure Gradient", *AIAA Journal*, American Institute of Aeronautics and Astronautics, Reston, Virginia, Vol. 7, No. 9, 1969, pp. 1752-1759.

18. Morgan, J.M., Wagner, G.A. and Wickens, R.H., "A Report on the Flight Dynamics of the Fokker F-28 Mk1000 as they Pertain to the Accident at Dryden, Ontario, March 1989", National Research Council Canada, Ottawa, Ontario, NRCC/NAE Report MISC 64, November 1989.

19. D'Avirro, J., Chaput, M., Hanna, M. and Flemming S., "Aircraft Full-Scale Test Program for the 1996/97 Winter", Transport Canada, Transportation Development Centre, Montreal, Quebec, TP13130E, December 1997.